Published in final edited form as:
NMR Biomed. 2013 December ; 26(12): . doi:10.1002/nbm.3045.

Glutamate and Glutamine: A Review of *In Vivo* MRS in the Human Brain

Saadallah Ramadan[*,a], **Alexander Lin**[b], and **Peter Stanwell**[a]

[a]School of Health Sciences, Faculty of Health, Hunter Building, University of Newcastle, Callaghan NSW 2308, Australia

[b]Alexander Lin: Center for Clinical Spectroscopy, Department of Radiology, Brigham and Women's Hospital, Harvard Medical School, 4 Blackfan Street, HIM-820, Boston MA 02115

Abstract

Our understanding of the roles that the amino acids glutamate (Glu) and glutamine (Gln) play in the mammalian central nervous system has increased rapidly in recent times. Many conditions are known to exhibit a disturbance in Glu-Gln equilibrium and the exact relationship between these changed conditions and these amino acids are not fully understood. This has led to increased interest in Glu/Gln quantitation in the human brain in an array of conditions (e.g. mental illness, tumor, neuro-degeneration) as well as in normal brain function.

Accordingly, this review has been undertaken to describe the increasing number of *in vivo* techniques available to study Glu and Gln separately, or pooled as 'Glx'. The present range of magnetic resonance spectroscopy (MRS) methods used to assess Glu and Gln, vary in approach, complexity and outcome, thus the focus of this review is on a description of MRS acquisition approaches, and an indication of relative utility of each technique rather than brain pathologies associated to Glu and/or Gln perturbation. Consequently, this review focuses particularly on (1) one-dimensional (1D) ^{1}H MRS, (2) two-dimensional (2D) ^{1}H MRS, and (3) 1D ^{13}C MRS techniques.

Keywords

Human; *in vivo*; Glutamate; Glutamine; MRS; ^{13}C; one-dimensional; two-dimensional

1. Introduction

Magnetic resonance spectroscopy (MRS) is a powerful technique to study endogenous metabolites in the human brain non-invasively *in vivo*. Traditionally, MRS studies have focused on the clinical context, but more recently there is also an increasing interest in research applications. With the advent of higher magnetic field strength scanners and an increasing sophistication of acquisition techniques and improved spectral resolution, there is now much interest in the study of metabolites that traditionally constitute one pool due to striking structural similarity within the human brain. This is especially true of the amino acids glutamine (Gln) and glutamate (Glu). Both Glu and Gln are relatively abundant amino acids in the human brain being in concentrations of 6-13 mmol $kg^{-1}{}_{ww}$ and 3-6 mmol $kg^{-1}{}_{ww}$, respectively (1).

[*]Correspondence to: School of Health Sciences, Faculty of Health, Hunter Building, University of Newcastle, Callaghan NSW 2308, Australia, saad.ramadan@gmail.com.

Our current understanding of the role of Gln and Glu has increased rapidly in recent times. Metabolically, Glu is stored as Gln in glia, and the balanced cycling between these two neurochemicals is essential for normal functioning of brain cells. Glu and Gln are compartmentalized in neurons and glia, respectively, and this chemical inter-conversion reflects an important aspect of metabolic interaction between these two types of cells. Glu, the most abundant excitatory neurotransmitter in the human brain, also plays a major role in synapsis where it is released from pre-synaptic cells, and then binds to post-synaptic receptors thus inducing activation.

In vivo studies have revealed that the neuronal/glial Glu/Gln cycle is highly dynamic in the human brain and is the major pathway of both neuronal Glu repletion and astroglial Gln synthesis (2,3). After its release into the synaptic cleft, Glu is taken up by adjoining cells through excitatory amino acid transporters (EAAT). Astrocytes are responsible for uptake of most extracellular Glu via the high-affinity Glu transporters GLT1 and GLAST and additionally have a vital role in preserving the low extracellular concentration of Glu needed for proper receptor-mediated functions, as well as maintaining low concentrations of extracellular Glu to prevent excitotoxicity (4,5). Once taken up into the astrocyte, Glu (along with ammonia) is rapidly converted to Gln by the astrocyte-specific enzyme Gln synthetase that is largely restricted to this cell type. Small quantities of Gln are also produced de novo or from GABA (6,7). Gln is released from astrocytes, accrued by neurons and converted to Glu by the neuron-specific enzyme phosphate-activated glutaminase (7). Gln is the main precursor for neuronal Glu and GABA (6), but Glu can also be synthesized de novo from tricarboxylic acid (TCA) cycle intermediates (8). The rate of Glu release into the synapse and subsequent processes are dynamically modulated by neuronal and metabolic activity via stimulation of extrasynaptic Glu receptors and it has been estimated that the cycling between Gln and Glu accounts for more than 80% of cerebral glucose consumption (9). The tight coupling between the Glu/Gln cycle and brain energetics is largely tied to the nearly 1:1 stoichiometry between glucose oxidation and the rate of astrocytic Glu uptake. This relationship was first determined by Magistretti *et al.* in cultured astroglial cells where the addition of Glu resulted in increased glucose consumption (10). These results provided the hypothesis that glycolysis in astrocytes results in a production of 2 molecules of ATP which are then consumed by the formation of Glu from Gln which suggests a tight coupling between the two mechanisms.

The role of Glu becomes more complicated when we consider that Glu is the metabolic precursor of γ-aminobutyric acid (GABA), the main inhibitory neurotransmitter in the mammalian cerebral cortex. This reaction is catalyzed by Glu decarboxylase, which is most abundant in the cerebellum. Glia obtain their Glu from the extracellular space, combine it with one molecule of ammonia, and convert it to Gln via the Gln synthetase pathway (11). This is the only brain region where Glu is converted into Gln. Glu is also the precursor to glutathione (GSH) and a building block of proteins (7,12). A thorough review of the metabolism of GABA and Glu in the human brain can be found in Petroff *et al.* (13).

The molecular structures of Glu and Gln are very similar and, as a result, give rise to similar magnetic resonance spectra (Figure 1). Thus, even though Glu has a relatively high concentration in the brain, its spectral features are usually contaminated by contributions from Gln, GABA, GSH and N-acetylaspartate (NAA). To avoid confusion in spectral assignment of Glu and Gln, a term ‘Glx’ has traditionally been used to reflect the combination of Glu and Gln concentrations (i.e. Glx = Glu + Gln). However, this approach does not allow for the evaluation of conditions where the concentrations of Gln and Glu are in opposing directions, nor does this approach allow for the evaluation of Gln and Glu separately.

As our understanding of the importance of Glu/Gln system in the human brain has increased, much endeavor has been invested in being able to quantify Glu or Gln separately. Biochemically, Glu plays a central role in many pathologies including pain perception (14), psychiatric diseases (15), epilepsy (16), Alzheimer's Disease (17), bipolar depression (18), mood disorders (19), ageing (20), and many others. Accordingly, there is now an array of MRS methods capable of studying and quantifying Glu and Gln separately and these vary in approach and outcome. This review contains descriptions of existing *in vivo* detection methods, with particular emphasis on (1) one-dimensional (1D) ^{1}H MRS (2) two-dimensional (2D) ^{1}H MRS, and (3) 1D ^{13}C MRS techniques.

2. Abnormalities in Glu/Gln Concentrations

The important role of neuroenergetics and Glu-Gln cycling in the pathogenesis of brain disease is being increasingly recognized. In this section, examples of diseases and normal physiologic events that involve Glu and Gln alteration as assessed with *in vivo* MRS are discussed. *In vivo* MRS has been used to demonstrate changes in the concentrations of Glu and Gln in the normal brain (21,22) as well as in a wide range of neurological and psychiatric diseases, including aging (23), depression and mood disorders (19,24), epilepsy (25,26), genetic disorders (27), hepatic encephalopathy (28-30), brain tumors (31-33), tumefactive multiple sclerosis lesions (34), alcohol addiction and drug abuse (35,36), schizophrenia (37,38) traumatic brain injury (39,40) and neurodegenerative disorders (41,42).

MRS studies of healthy volunteers have demonstrated significant changes in both GABA and Glu in specific brain regions accompanying brain maturation as well as heterogeneity in brain structures (21,22,43), while differences in Glu and Gln concentrations in gray and white matter have been noted (12). Alterations of Glu, specifically elevated Glu/NAA ratio in gray matter (GM) with normal Glu/NAA in white matter (WM), has been reported in subjects with Rett's syndrome compared with controls (27), while elevations of Gln have been demonstrated in hepatic encephalopathy (HE) and Reye's syndrome (44). In HE, ammonia is produced and transported through the bloodstream into the brain. One of the functions of the Glu-Gln cycle is the removal of damaging ammonia via increased Gln synthase in the astrocyte. Gln expression has additionally been shown to increase under hyperammonemic conditions (45); and elevated Gln has been detected in patients with cirrhosis of the liver, where the brain is exposed to chronically elevated ammonia in the blood as a result of liver failure. Neurospectroscopic alterations have been reported with increase in the Glx/creatine (Cr) ratio accompanied by decrease in myo-inositol (mI)/Cr ratio and total choline (tCho)/Cr ratio in liver disease (30,46,47). Moreover, the extent of the MRS alterations in these patients can be observed subclinically (48) and increases with increasing grade of HE (28), with reversibility of these changes being reported following liver transplantation (29,49). The temporal resolution of Glx/Cr to reach normal levels is within 1–2 months, except for those patients with higher pre-transplant values that may take longer (29). Moreover, the normalization of spectroscopic abnormalities often precedes the temporal resolution of pallidal hyperintensity on MR imaging which may take up to 12 months (30).

MRS studies of primary brain tumors have also reported significantly increased Glx in oligodendrogliomas compared to astrocytomas (50,51). It has been reported that the metabolic profile of oligodendrogliomas shows an increased level of Glx (as well as a decreased level of NAA and increased levels of choline-containing compounds) compared with WM and the level of Glx was significantly higher in low-grade oligodendrogliomas than in low-grade astrocytomas and may serve as a metabolic marker in diagnosis and treatment planning. As well, concentrations of total Glx (as well as choline, and lactate +

lipid) have been reported to be higher in high-grade compared to low-grade gliomas (32,52). Glx has additionally been reported to be diagnostic in the differentiation of meningiomas from other intracranial lesions (31,53). Glx is also elevated in multiple sclerosis (MS) and has also been reported as elevated in tumefactive appearing MS lesions (34), while it reduced in cortical gray matter in the chronic course of primary progressive MS.

As Glu is the main excitatory neurotransmitter in the human brain it is believed to play an important role in the initiation, spread, and maintenance of epileptic activity (25). MRS has provided evidence of reduced metabolism in brain regions affected by epilepsy that indicates alterations in neuroenergetics (54). Furthermore, chronically elevated extracellular Glu has been found in epileptogenic sclerotic tissue, and growing evidence now indicates that interictal energetic deficiency in the epileptogenic hippocampus contributes to impaired Glu reuptake and Glu-Gln cycling that results in chronically elevated extracellular Glu, glial and neuronal toxicity, increased lactate production together with poor lactate and glucose utilization, that results in deterioration in energy metabolism (26). Additionally, ^{13}C MRS studies of neurosurgical specimens have revealed marked impairment in Glu/Gln cycling compared with more histologically normal tissue (13).

There is also emerging evidence that abnormalities in glutamatergic neurotransmission may underlie psychopathological phenomena observed in schizophrenia (37,38), major depression disorders and bipolar disorders (19,24), and alcohol addiction (35). Moreover, it has been proposed that the Glu metabolite pool relevant to neurotransmission is constricted in major depressive disorders but expanded in bipolar disorder (19). It should be noted however, that there are also contrary reports that may be dependent on the methods used in the study. Similarly, drug abuse studies undertaken using MRS have identified alterations in Glx (as well as NAA, mI, and tCho) that suggest that drugs of abuse may affect neuronal health, neuroenergetics and neurotransmission, inflammatory processes, and cell membrane turnover that may underlie the neuropathology that give rise to the cognitive and behavioral impairments related to drug addiction (36).

Mitochondrial dysfunction has been implicated in the loss of brain function in neurodegenerative disease and normal aging (55) leading to increased Glu (56). ^{13}C MRS has revealed alterations in glutamatergic neurotransmission and neuroenergetics that are consistent with the view of impaired glutamatergic neurotransmission contributing to the underlying cause of Alzheimer's disease (AD) (41). Moreover, a recent MRS study comparing groups of healthy elderly with young adult subjects was able to demonstrate a reduction in neuronal mitochondrial metabolism and diminished Glu–Gln cycling in elderly compared with young subjects (57). These results were interpreted as consistent with the assertion that mitochondria lose oxidative capacity with advancing age, leading to a loss of brain function (57).

3. MRS Detection Techniques *in vivo*

3.1. 1D ^{1}H MRS techniques

There are a number of 1D ^{1}H MRS methods that are reported in published literature to detect and/or evaluate Glu and/or Gln, or Glx in humans *in vivo*. The following is a description and evaluation of the different categories of methods:

1. Detection of Glx with 1H MRS

Localized single voxel spectroscopy is the simplest technique for the *in vivo* detection of Glx. Prost *et al*. compared *in vivo* detection of Glx using a standard PRESS sequence at magnetic field strengths of 0.5 and 1.5 Tesla in a group of eight healthy volunteers (58).

They reported that the resonances of Glx at 0.5 Tesla had two times the signal-to-noise ratio (SNR) compared to Glx recorded at 1.5 Tesla. This is due to the chemical shift difference between C3 and C4 protons at 0.5 Tesla decreasing, and as a result the ratio of δ/J approaches zero, leading to coalescence of resonances of protons on C3 and C4 to a single resonance, thus resulting in a well separated Glx resonance separate from NAA resonances.

When spectra were acquired at 0.5 and 1.5 Tesla, using a $2\times2\times2cm^3$ voxel in the right front-parietal cortex (TR=1.5s, TE=41ms, acquisition bandwidth of 1000 Hz) and analyzed, a pseudo-singlet for Glx was identified at 2.35ppm at 0.5 Tesla, whereas at 1.5 Tesla a very complicated multiplet was observed for Glx. In this study the Glx/Cr ratio determined from spectra measured at 0.5 Tesla was 1.00±0.07 (58). The spectral simplicity of Glx acquired at 0.5 Tesla is an important feature of this method.

2. TE-averaged PRESS

In this method, a number of 1D PRESS spectra are acquired at variable TE values, and co-added (averaged) in real time to produce a single 1D, TE-averaged spectrum. Alternatively, the same TE-averaged spectrum can be obtained if these time-domain FIDs are ordered in a 2D matrix and a two-dimensional Fourier transform (2DFT) applied. The resultant 1D spectrum corresponding to the middle of the F1 axis (F1=0 Hz) is equivalent to the TE-averaged spectrum obtained above (59,60). This 1D spectrum offers relatively uncontaminated spectral peaks for C4 protons at 2.35ppm for Glu, and for C2 protons at 3.75ppm for Glx (61). Thus, acquiring 128 steps with an increment time of 2.5ms, and 2 averages per increment with an initial TE=35ms yields a TE-averaged spectrum with peaks representing Glu and Glx at 2.35 and 3.75ppm, respectively. Gln levels can be estimated as the difference between Glx and Glu resonances.

Using a TE-averaging method, and correcting for T1 and T2 relaxation, Hurd *et al.* (61) was able to determine Glu and Gln concentrations of 7.1±0.5 mmol $kg^{-1}{}_{ww}$ and 1.7±1.6 mmol $kg^{-1}{}_{ww}$ in WM and 11.7±1.1 mmol $kg^{-1}{}_{ww}$ and 3.2±1.6 mmol $kg^{-1}{}_{ww}$ in GM. A spectral basis set for Glu and Gln estimation using identical acquisition parameters as used in the *in vivo* acquisition, was simulated using GAMMA (62) and was used for spectral fitting in this experiment.

While TE-averaging is a simple and reliable method for measuring Glu and Gln, it sacrifices spectral information arising from the J-evolution of other metabolites. The method also suffers from differential T2 weighting per individual TE value, which can be corrected for if a basis set is similarly simulated or experimentally acquired. TE-averaging sequences are not usually available from major MRI vendors but can be easily modified from standard PRESS sequence source code.

3. TE-averaged two-dimensional proton magnetic resonance spectroscopic imaging (TE-averaged MRSI)

This method is similar to the above TE-averaging method, but it is applied to multiple voxels in a spectroscopic imaging mode (63). In an MRSI study by Srinivasan *et al.*, a data array of 10x16 voxels was acquired on a 3 Tesla magnet in 21 minutes using a flyback echo planar gradient trajectory in the anterior–posterior (AP) direction for phase encoding, with 64 echo time steps starting at TE=35ms with an echo time increment of 2.5ms. In this study, Glu concentrations were corrected for T1 relaxation to account for saturation effects, but not for T2 relaxation effects as Glu does not follow a single or bi-exponential curve with multiple echo times. Spectral quantification of Glu at 2.35ppm was performed using LCModel after acquiring basis spectra from a phantom with known concentrations of relevant metabolites. Gln was not quantified using this approach. From the processed MRSI

spectral map, it was found that Glu is more abundant in GM (9.4±1.0 mM) relative to WM (4.5±0.6 mM), as reported previously (64,65). The advantage of this approach is that whole brain coverage is possible; however, acquisition sequence implementation and data analysis are complicated by a lack of standard software packages and vendor support.

4. Optimal TE for Glu and Gln detection

Schubert *et al.* (66) were able to selectively detect C4 proton resonances of Glu using a PRESS sequence at 3 Tesla with a TE=80ms and analyzing the data using both the time and frequency domains with prior knowledge obtained from phantom spectra. Using this approach, *in vivo* spectral features were similar to *in vitro* Glu spectral features collected from a phantom, and Glu signal was well resolved and separated from major interferences, including Gln and NAA. Schubert *et al.* (66) reported that *in vivo* data acquired from the anterior cingulate cortex (ACC, voxel size: $2.5\times4\times2cm^3$) and hippocampus (voxel size: $2\times3\times2cm^3$) had concentrations of Glu and Gln in the ACC of 11.7±1.2 and 2.5±0.8 mM, respectively, while in the hippocampus Glu and Gln were found to be 10.9±1.4 and 2.2±0.8 mM, respectively (66).

Similarly, Jang *et al.* acquired PRESS spectra at 1.5 Tesla *in vitro* and *in vivo* at four TE values: 30, 35, 40, and 144ms (67), with resulting spectra analyzed with LCModel (68). For both in vitro and *in vivo* conditions, spectra yielded the lowest Cramer–Rao Lower Bounds (CRLB) for Glu quantitation when TE was set to 40ms. Additionally, Jang *et al.* (67) reported results from *in vivo* spectra acquired using a $2\times2\times1cm^3$ voxel located in the ACC, with NEX of 128 and TR of 2s from 21 healthy subjects, where a Glu concentration of 10.51±1.16 mM, and a Gln concentration of 4.70±1.00 mM were found. Similar results were reported from spectra acquired from the insula.

Furthermore, Mullins *et al.* (69) compared TE-averaged, TE=40ms, and TE=30ms PRESS spectra collected *in vitro* and *in vivo* at a magnetic field strength of 3 Tesla and found that the TE=40ms PRESS sequence gave the lowest CRLB, in agreement with Jang *et al.* (67) for an *in vivo* voxel ($2\times2\times3cm^3$) positioned in the ACC. Furthermore, they reported a Glu concentration of 13.14 mM (CRLB=8%) and a Gln concentration of 2.35 mM (CRLB=29%).

TE optimization for the purposes of Glu and Gln detection has also been demonstrated using stimulated echo acquisition mode (STEAM) spectroscopy by Yang *et al.* (70), who optimized TE and mixing time (TM) to resolve the C4 proton resonances of Glu (2.35ppm) and Gln (2.45ppm). In this study, spectra were simulated and data acquired *in vitro* and *in vivo* at 3, 4, 4.7, 7, and 9.4 Tesla. The combination of greatest resonance amplitude and resonance separation was found at (TE, TM) of (72ms, 6ms), (82ms, 48ms), (82ms, 94ms), (74ms, 68ms), and (80ms, 84ms) at magnetic field strengths of 3, 4, 4.7, 7, and 9.4 Tesla, respectively Additionally, Yang *et al.* (70) reported , a Glu concentration of 10.00±0.69 institutional units with a CRLB of 12.25±2.65, while Gln concentration was 5.54±0.55 with a CRLB of 19.37±4.40. In this study spectra were collected from the medial occipito-parietal junction from six healthy volunteers at 3 Tesla and data analyzed using LCModel (70).

Optimal TE methods are appealing acquisition strategies due to their ease of implementation for both acquisition and processing and the ease with which appropriate parameter timings can be selected at the scanner interface. Additionally, resulting spectra can be analyzed using scanner software or commercially available software (e.g. LCModel, jMRUI) after simulating an appropriate basis set.

5. Glu amine group-water **C**hemical **E**xchange **S**aturation **T**ransfer (GluCEST)

Chemical exchange saturation transfer (CEST) is a sensitivity enhancement technique that is able to indirectly detect metabolite content based on their exchange-related properties (71). CEST utilizes the reduction of the bulk water magnetization due to the exchange of saturated magnetization from exchangeable protons of solute metabolites with bulk water. This reduced magnetization manifests as image contrast due to the metabolite. This technique was recently implemented by Cai *et al.* where the chemical exchange saturation transfer (CEST) between bulk water and Glu was utilized for detection of Glu (72). Cai *et al.* demonstrated that Glu exhibits a concentration dependent CEST effect (GluCEST) between its amine ($-NH_2$) and bulk water protons. Glu amine protons have an exchange site at approximately 3.0ppm from water and the CEST effect from glutamate is linearly proportional to the Glu concentration in the physiological pH range. Since this is an imaging technique, the Glu concentration is represented on a color-coded image reflecting the variable concentration of Glu in brain. In the human brain at 7 Tesla *in vivo*, the GluCEST technique observed the Glu gray matter to white matter ratio to be 1.6±0.2 (72). An excellent review of chemical exchange methodology can be found here (73).

The GluCEST approach has promising potential as it offers good spatial and temporal resolutions and covers a full brain slice to yield a color map reflective of Glu concentration. Additionally, Gln has no contribution to the final signal, and thus cannot be quantified using this technique. Cr, GABA and macromolecules represent a significant contamination source to the detected Glu signal, and thus need to be factored into spectral analysis to improve the accuracy of this technique. The proposed technique is relatively new, even though the concept of chemical exchange is not. Clinical implementation is not straightforward due to a high level of expertise required to acquire and process data.

6. Very short echo time (TE: 6ms, 6.5ms) MRS

Short TE acquisitions are preferred to long TE acquisitions in strongly coupled spin systems, such as Glu and Gln, as they limit peak phase modulation. A short TE approach in such coupled systems gives rise to spectra where the majority of peaks are in-phase and with reduced signal cancellations due to J-modulations inherent at longer echo times. This in turn results in more robust signal quantification. Wijtenburg *et al.* (74) determined Glu/tCr at 3 Tesla by combining short TE STEAM (6.5ms) with phase-rotation (75,76) to detect Glu in human brain. This short TE approach has also been compared to 40ms TE PRESS, 72ms TE STEAM, and TE-averaging with spectral analysis performed using the LCModel software package (68). The Glu/tCr ratios as well as coefficient of variations (CV) were determined for all methods. It was found that short TE phase-rotation-STEAM approach yielded the greatest precision for Glu/tCr ratio quantification (1.12±0.08; CV=7.1%), followed by TE-averaging (1.01±0.09 (CV=8.9%)), PRESS 40ms (1.09±0.13; CV=11.9%), and STEAM 72ms (1.23±0.17; CV=13.8%)(74).

Additionally, Mekle *et al.* used a SPin ECho, full Intensity Acquired Localized (SPECIAL) spectroscopy sequence at 3 Tesla with a TE=6ms to acquire data from a $2\times2\times2cm^3$ voxel located in the occipital lobes of six healthy volunteers (77). Spectra acquired using the SPECIAL approach revealed no baseline distortions. Concentrations of Glu and Gln obtained using LCModel analysis were (8.9±0.9 mmol/kg, %CRLB=3±0.5) and (1.6±0.4 mmol/kg, %CRLB=13±4.4), respectively. It is noteworthy to mention that the SPECIAL sequence is an add-subtract sequence that is based on a combination of image-selected *in vivo* spectroscopy(ISIS) (78) and spin-echo sequence.

The implementation of very short echo time techniques requires substantial modification of standard vendor supplied localization sequences. As well, these spectra are usually complicated by a broad baseline extending over the whole spectral width and care should be

taken during analysis to eliminate the contribution of the baseline to the desired metabolite signal- which is achieved by utilizing T1 differences (79). The use of third party spectral analysis software, and in some cases, the collection or simulation of metabolite basis sets, are essential to yield results of high accuracy (74).

7. Glu and Gln at high magnetic fields (4 and 7 Tesla)

The use of high magnetic field strengths, and the inherent associated increased spectral resolution, can increase the precision in quantifying Glu and Gln separately. Garwood *et al.* (80) reported Glu and Gln concentrations in parietal white matter ($8cm^3$ voxel, n=10) to be 5.47±0.56 and 1.92±0.35 mM, respectively, whereas in the posterior hippocampus Glu and Gln were found to be 7.67±2.39 and 4.08±2.14 mM, respectively. Data were acquired at 4 Tesla using a LASER sequence (TE=46ms) with analysis using a linear combination fitting technique with corrections for contributions from macromolecules (81).

Similarly, Tkac *et al.* implemented a short TE STEAM sequence (TE=6ms, TM=32ms) and reported Glu concentration of 9.1 μmol/g (CRLB<5%), and Gln concentration of 3.3 μmol/g (CRLB<5%) for spectra collected from the occipital lobe of 10 healthy volunteers at 7 Tesla (82,83). While, Mangia *et al.* implemented, in a functional MRS mode, a STEAM sequence (field strength 7 Tesla, TE=6ms, TM=32ms, 128 scans, TR=5s, 12 healthy subjects, voxel size=20×22×20 mm^3) to measure the change in Glu concentration, and other metabolites, in the visual cortex after paradigms of visual stimulations (84). Glu was found to increase by +3±1% ($P < 0.01$) upon stimulation compared to the resting phase. The same group used 'SPECIAL' spectroscopy sequence with a TE=6ms at 7 Tesla to acquire data from voxels located in the occipital lobes (77) or the primary visual cortex (85) of six healthy volunteers. Occipital lobe concentrations of Glu and Gln obtained using LCModel analysis were found to be (9.9±0.9 mmol/kg, %CRLB=1.1±0.5) and (2.2±0.4 mmol/kg, %CRLB=4±1.1), respectively (77). In the primary visual cortex, Glu and Gln were found to be 9.6±0.2 and 2.3±0.1 μmole/g, respectively, with 4% increase in Glu concentration upon visual stimulation (85).

Furthermore, Emir *et al.* (86) used a 16-channel transceiver on a 7 Tesla human magnet with an optimized shimming algorithm, and acquired data from seven different brain locations. LCModel analysis revealed that the lowest Glu level was in the substantia nigra (5.9±0.5 μmol/g) and the highest Glu level in the posterior cingulate cortex and putamen (10.8±0.5 and 10.7±0.3 μmol/g, respectively). These results were obtained in 14 healthy volunteers using a STEAM sequence (TR=5s; TE=8ms; TM=32ms). More results are shown in Table 1.

While all the above methods are echo based, Henning *et al.* developed a FID based MRSI technique where data acquisition starts after applying a single slice selective radio frequency (RF) pulse preceded by water suppression and outer volume suppression pulses at 7 Tesla(87). This technique was used to generate Glu and Gln spectral maps, however, no quantitation was attempted in the human brain (87).

Improved hardware design, B_1 homogeneity, shimming capabilities, and short TE MRS sequences enable more accurate quantification of Glu in the human brain at high magnetic field strengths (82,86). Consequently, higher magnetic field strength is preferred for MRS measurements due to greater inherent chemical shift dispersion and improved SNR. However, suitably designed RF pulses that can cover a relatively large bandwidth without overloading the RF amplifier, optimized shimming techniques, and local transceiver coils are essential for improved results.

8. Difference spectroscopy

Double-resonance difference spectroscopy is a technique that was initially implemented in rat brain *in vivo* in 1984 (88). This technique was later optimized for localization in humans by Mescher *et al.* (89) in 1998 and developed for GABA editing, becoming widely known as MEGA-PRESS. In this technique, alternate scans are usually acquired with RF pulses centered on- and off-resonance with respect to the chemical species that is coupled to the resonance to be edited, with a TE≈73ms. Upon subtraction of these alternate scans, the residual signal corresponds to the edited GABA resonance at 3.0ppm and co-edited Glu signals at 2.3 and 3.75ppm.

Using this approach Waddell *et al.* (90) determined the Glu/tCr ratio in ACC and cerebellar vermis to be 1.16±0.10 and 0.7±0.07, respectively. While Lee *et al.* (91) also used a similar method where they eliminated J-modulation by using a TE value less than 1/4J and used spectral subtraction at two different TE values to quantify Glu at 1.5 and 4 Tesla. They reported optimal TE values at 1.5 and 4 Tesla to be 30/42ms and 20/40ms, respectively. They also noted that NAA and GABA contributed to the final Glu signal (91). No attempt to quantify Glu or Gln *in vivo* was attempted, even though phantom studies showed a linear correlation between edited spectra and phantom concentrations.

Additionally, Snyder *et al.* were able to selectively detect Glu and suppress Gln, *in vivo*, by subtraction of spectra acquired at constant TE but with different inter-echo timings (PRESS asymmetry) at 4.7 Tesla (92). The subtraction of two PRESS spectra acquired from a $1.5\times1.5\times1.5 cm^3$ voxel in parietal GM with interpulse delays of (TE1=80ms, TE2=75ms) and (TE1=125ms, TE2=30ms) yielded a pure Glu signal at 2.0–2.3ppm. No quantification was attempted in this approach (92). This approach was originally proposed by Gambarota *et al.* to detect the citrate resonance in prostate (93).

Difference spectroscopy is popular due to its conceptual simplicity and ease of implementation. For these reasons this approach is widely used for selective editing to quantify Glu and Gln, and subsequent correlation of the edited spectrum with spectra acquired from phantoms with known Glu and Gln relaxation properties and concentrations. However, due to the long TE value needed to accommodate frequency-selective inversion pulses, there is considerable attenuation of various chemical species, leading to low inherent SNR.

9. Optimized interpulse delays in PRESS sequence from 1.5 Tesla to 7 Tesla

PRESS sequence timing can be written as: 90° TE1/2 180° TE1/2 TE2/2 180° TE2/2 acquire, with TE=TE1+TE2. J-modulation as a function of TE impacts adversely on resonance signal amplitude in strongly coupled metabolites such as Glu and Gln. Accordingly, Snyder *et al.* (94) revealed that different combinations of TE1 and TE2 resulted in different peak overlap and peak amplitude for the CH2 groups of Glu at 2.33–2.35ppm, and 2.43–2.45ppm for Gln. Simulations at 1.5, 3, 4.7 and 7 Tesla field strengths yielded [TE1=TE2=55ms], [TE1=30ms, TE2=85ms], [TE1=20ms, TE2=90ms], and [TE1=20ms, TE2=85ms], respectively, as optimal TE1/TE2 combinations that give maximum Glu-Gln peak separation and amplitude in the 2.3–2.6ppm range. Further, *in vivo* evaluation performed at 4.7 Tesla, resulted in reasonable peak resolution and separation of Glu and Gln using the above determined TE1/TE2 timings (94). No quantification was attempted in this work. The proposed method is attractive in its ease of implementation; however, more work is needed to correlate detected peak areas with metabolite concentration.

10. Carr-Purcell PRESS (C-PRESS)

C-PRESS is a sequence where two additional shaped refocusing RF pulses are inserted between the two traditional refocusing RF pulses of PRESS sequence. Reports have compared the performance of PRESS (TE=35ms), C-PRESS (TE=45ms) (95) and TE averaged PRESS (TE-averaged, TE=35–192.5ms) (61) for the evaluation of *in vivo* Glu (96,97). It was reported that:

i) longer TE PRESS yields more accurate Glu concentrations, and

ii) Glx is best detected at a 144ms TE PRESS sequence (which is not optimal for Glu).

Both short TE C-PRESS and short TE PRESS sequences result in more repeatable Glu measurements, while slightly overestimating the Glu concentration, while TE-averaged PRESS method produced higher coefficients of variation and CRLB than both short TE PRESS and C-PRESS sequences (97).

The C-PRESS approach is simple but requires a reasonable level of pulse sequence development to obtain more repeatable Glu measurements.

11. Measurement of Glu and Gln by spectrally-selective refocusing at 3 Tesla

The chemical shift separation between the protons on C4 groups on Glu and Gln molecules is 0.1ppm, equivalent to 13Hz at a magnetic field strength of 3 Tesla. This difference can be exploited by means of spectrally-selective refocusing using a long Gaussian RF pulse to detect Glu or Gln selectively (98). When a Gaussian pulse is inserted between the two 180° RF pulses of a PRESS sequence, a sequence written as: 90° 180° Gaussian 180° acquire is obtained, with a full width at half maximum of the Gaussian pulse of 12.0 Hz. Thus, at magnetic field strength of 3 Tesla, to detect Glu, a triple resonance Gaussian pulse (82ms) can be utilized for refocusing Glu at 2.35ppm, and Cr at 3.02ppm and 3.92ppm at a TE value of 128ms. Similarly, to detect Gln, a triple resonance Gaussian pulse (90ms) can be utilized for refocusing Gln at 2.51 (Gln), and Cr at 3.02ppm and 3.92ppm for a TE value of 158ms. In this approach, the signal for Cr is used for signal referencing. Both approaches have been shown to produce well resolved C4 target multiplets in separate experiments with minimal contamination from NAA and GSH. Using the above method, the concentrations of Glu and Gln in the prefrontal cortex were estimated to be 9.7±0.5 and 3.0±0.7 mM (mean±SD, n=7), with reference to Cr at 8 mM (98).

The editing nature of this technique means that only Glu or Gln can be acquired in a single measurement, but not both at once. Also, the long TE employed in these approaches yield a flat baseline with little or no contribution from macromolecules. However, because of the very narrow separation of peaks of interest (13Hz), minor frequency drifts can be detrimental to this approach. A reasonable level of sequence programming expertise is required to implement this approach in a clinical environment.

12. Proton Echo-Planar Spectroscopic Imaging (PEPSI)

PEPSI is a technique that acquires MRSI data in the presence of an EPI readout gradient, and thus, has the ability to cover a large field of view in a relatively short period of time (99,100). This technique can be used in conjunction with parallel imaging techniques such as SENSE (101,102) or GRAPPA (103) to achieve further gains in measurement time. Recently, this approach has been used to study J-coupled resonances in the brain, using a square FOV of 26×26cm^2, 32×32 pixels, 1.5cm slice thickness, TE 15ms, and TR 2s and total acquisition time of 8.5 minutes to provide separate metabolite images for metabolites of interest (99,100). Using this approach, Posse *et al.* (99,100) found Glu concentration to be significantly higher in GM compared to WM. Additionally, the concentrations of Glu and

Glx were mapped with mean CRLBs less than 18%. Gln was detected with greater sensitivity at 4 Tesla compared to 3 Tesla, but was limited by SNR thus yielding high CRLBs (38%), with a slice-averaged Gln concentration of 2.7 mM. Moreover, at 3 Tesla, concentrations of Glu in GM and WM were found to be 12.8±1.5 mM and 7.0±1.1 mM, respectively. At 4 Tesla, concentrations of Glu in GM and WM were found to be 11.9±1.9 mM and 5.0±1.2 mM, respectively (99,100). This type of acquisition, while appealing in its coverage and reliability, is challenging to implement as it requires specialized acquisition, processing and analysis.

13. Detection of Glu using Double Quantum Filter

A double quantum filter ($90°_{ss}$ $180°_{ss}$ 90_{hd} $90°_{ss}$ $180°_{ss}$ acquire, ss: slice selective , hd: hard) has previously been described for the detection of Glu (104). In this study by Thompson *et al.*, the 2.3ppm peak of Glu was identified as the target resonance, and the performance of the double quantum filter was evaluated theoretically, in phantoms, and *in vivo* in human brain at 3 Tesla. Even though frequency separation between Glu and Gln in a standard 1D spectrum is not high enough to detect Glu alone, the proposed filter was able to detect the 2.3ppm Glu peak with minimal Gln contamination. No quantitative values for *in vivo* Glu were reported.

Another double quantum based method is spectroscopic imaging of Glu by water-suppressed J-refocused coherence transfer (105). In this method, a multiple quantum coherence transfer J-refocussed preparation serves to suppress water and refocus signal from strongly coupled spin systems such as Glu (105). The detection of Glu using this method relies on the detection of C4 methylene protons (resonating at 2.36ppm) adjacent to the COOH group in the Glu molecule. The pulse sequence is made out of a set of outer volume suppression pulses followed by a block of ISIS (78) RF pulses followed by a coherence transfer block consisting of hard RF pulses. Using this approach, a spectroscopic image was acquired with a 16x16 matrix and a FOV of 200×200 mm, with a nominal voxel size of 4 ml, TR of 2s and total acquisition time of 34 min. No Glu quantification was attempted in this study. This approach relies on high magnetic field strength to decrease the effects of strong coupling, high B_1 homogeneity and good phase coherence. Pulse sequence programming expertise, as well as calibration using known phantom concentrations, is required for clinical implementation.

An integral component of the majority of the above methods is quantification using linear combination of model spectra in single voxel as well as spectroscopic imaging techniques. Since a 1D spectrum is a combination of signals originating from many compounds, a technique was developed to analyze an *in vivo* spectrum by creating a similar spectrum made out of signals taken from a phantom or simulated spectral data base. LCModel, Linear Combination of Model spectra of metabolite solutions *in vitro*, is a commercial software package that analyzes and quantifies *in vivo* spectra by comparing them to a synthesized set of pure metabolite spectra (68,106,107). LCModel contains a “basis set” that is either acquired in phantoms or simulated using GAMMA software (62) and is composed of individual spectra of various metabolites acquired at a certain TE that matches the experimental TE and magnetic field strength used *in vivo*. Additionally, the program also takes into account baseline distortions due to the broad macromolecule resonances. Thus, from the time-domain input, and the frequency domain combination, LCModel produces estimates of absolute concentrations (in mM) or ratios to total creatine of each metabolite and their uncertainties (standard deviation and Cramer-Rao lower bounds). The method has been applied to STEAM and PRESS acquisitions for both in single voxel and multi-voxel modes. Gussew *et al.* (107) used LCModel to determine the Glu concentration in the anterior insular cortex of healthy volunteers and reported a concentration of 8.9±0.6 mM

(single voxel, PRESS sequence, TE 30ms). Gln, however, has always been determined with higher uncertainty due to its low concentration. MRSI data have also been processed by LCModel to produce Glu concentrations in different parts of the brain (108). Since basis sets can be simulated, LCModel can be used to analyze data acquired from any pulse sequence as along as the basis set used for quantification is simulated with a matching pulse sequence.

jMRUI can also be used to quantify Glu and Gln, as well other metabolites, and uses prior knowledge spectral fitting methods to perform absolute quantitation in the time domain (84,109). jMRUI, however requires a higher degree of user input and expertise than LCModel. Comparison of LCModel and jMRUI capabilities has been reported elsewhere (84).

All the above methods are based on a 1D approach and take advantage of the scalar coupling properties of Glu and Gln. Since Glu is more abundant than Gln in normal human brain tissue (1), many sequences can only reliably detect the more abundant Glu signal and cannot accurately assess changes in Gln. Findings from all the above techniques are summarized in Table 1.

3.2. 2D ^{1}H MRS Techniques

In vivo 2D MRS was introduced by Aue *et al.* (110) in 1976 as a simple two hard RF pulse sequence ($90°_{x}$ t1 $90°_{x}$ Acquire, t1 is an incremented time delay) which, following 2D Fourier transformation, produced a 2D COrrelation SpectroscopY (COSY) spectrum, which can be used to confirm chemical structure. Another two-hard RF pulse sequence that was also introduced by Aue *et al.* was J-resolved spectroscopy ($90°_{x}$ t1/2 $180°_{x}$ t1/2 Acquire, t1 is an incremented time delay) which was originally proposed for homonuclear decoupling (111).

Fewer two-dimensional (2D) spectroscopic techniques have been developed to determine separate concentrations of Glu and Gln. Similarity between the 2D COSY and J-resolved spectroscopy profiles of Glu and Gln is striking (Figure 2, Figure 3), but 2D might offer an improved chance for detection and quantification due to the introduction of the second spectral dimension.

The majority of these 2D methods are based on fitting of model spectra and include the following:

1. ProFit at 3 Tesla

ProFit (Prior-Knowledge Fitting) (112) is a software package where 2D spectra can be analyzed to yield quantitative (relative to Cr) metabolite results. Two fitting algorithms are combined in ProFit:

i) linear combination of model 2D spectra, and

ii) VARPRO (variable projection) which is a parameterized fit in the time domain.

After an initializing fit, three fitting iterations using linear combination of 2D spectra and VAPRO are usually s ufficient to determine the components of a 2D spectrum and compute metabolite concentrations. Metabolites ratios to Cr are produced as well as their corresponding standard error estimates in the form of Cramer–Rao lower bounds (CRLBs). ProFit can be applied to all kinds of 2D experiments, but was originally implemented, tested and verified with localized J-resolved spectroscopy (JPRESS, 90° 180° t1/2 180° t1/2 Acquire, all RF are slice selective) due to the high SNR of this technique. Simulated basis spectra, produced with the same pulse sequence timings used experimentally, must be

generated for metabolite quantitation. Semi-quantitation of Glu and Gln has been undertaken *in vivo* in 27 healthy volunteers and yielded ratios of Glu/Cr=1.28 (%CRLB=2.6±0.4), and Gln/Cr=0.213 (%CRLB=13.6±2.4) (112). Additionally, Schulte *et al.* reported that Glu and Gln results obtained from ProFit were more accurate than those obtained from short TE 1D studies with spectral analysis using LCModel (112), however, the time taken to acquire JPRESS is longer than the time used to acquire 1D PRESS spectrum.

Localized correlation spectroscopy (L-COSY) (90° 180° t1 90° Acquire, all RF are slice selective) which has a terminal 90° RF instead of the terminal 180° RF pulse in JPRESS, was developed by Thomas *et al.* (113,114). Frias-Martinez *et al.* demonstrated that L-COSY acquired from the occipital lobe, and processed with a modified version of ProFit, produced lower CRLB values than JPRESS spectra (115). Comparative results are reported in Table 1.

Other types of localized COSY acquisitions (e.g. adiabatic COSY (116,117), CT-COSY (118)) may produce improved results for Glu and Gln evaluation but are yet to be evaluated using ProFit analysis.

2. J-resolved spectral fitting using 1D LCModel basis set 4 Tesla

Since a two-dimensional JPRESS spectrum is a series of 1D spectra acquired at equally separated TE intervals, a JPRESS dataset can be resolved into a series of one-dimensional spectra where each spectrum is modeled and fitted with its theoretically customized LCModel template. Metabolite levels are derived from the total integral across the J-series of spectra for each metabolite.

Using JPRESS, data obtained from phantoms containing physiologic concentrations of the major brain metabolites provided more accurate concentration estimates for common metabolites including Glu and Gln than 1D results (119). Jensen *et al.* (119) implemented localized JPRESS at 4 Tesla and compared the reproducibility of the J-resolved spectral fitting method against a TE 30ms PRESS method for Glu and Gln quantification with a voxel placed within the parieto-occipital cortex from one healthy volunteer repeated nine times. *In vivo* JPRESS (Glu/Cr: 0.90±6%, Gln/Cr: 0.25±14%) yielded superior reproducibility than 30ms PRESS (Glu/Cr: 1.24±8%, Gln/Cr: 0.17±30%) (119).

3. FiTAID, Fitting Tool for Arrays of Interrelated Datasets

FiTAID is based on 2D linear-combination model fitting of magnetic resonance spectra which offers enhanced features not available in other software packages such as fitting either in the time domain, in arbitrary spectral windows in the frequency domain, or in either domain according to arbitrary fit strategy steps. It also allows the user to fit limited parameter sets or limited parts of the 2D data matrix (120). This software package has also been successfully used to study the macromolecular baseline in ^{1}H MR spectroscopy. Though FiTAID has not been used to quantify Glu or Gln *in vivo*, the features of this software are theoretically capable of delivering successful implementation for this purpose.

4. Multi-TE J-resolved spectral fitting

This approach has been developed and compared to TE-averaging, as well as 1D PRESS (TE=30ms) methods by Gonenc *et al.* (121). In a successful implementation of the multi-TE approach, TE was varied from 30ms to 180ms in steps of 10ms, and resulting spectra were sorted into a 2D array, in contrast to TE-averaging where all spectra are co-added to yield one simplified 1D spectrum. It was found that the multi-TE J-resolved approach (Glu/Cr: 1.11±0.11, and Gln/Cr:0.43±0.08) yielded the lowest coefficient of variation when

compared to other methods (121). No absolute quantitation was attempted though it could be undertaken if an appropriate T2-corrected basis set was implemented.

5. Constant-time COSY techniques at 3 and 4.7 Tesla

This is similar to the L-COSY sequence described above, but the time delay between the first and last RF pulses is constant. This leads to the collapse of the scalar coupling effect along F1 dimension and to an improvement of peak resolution, apparent even in magnitude mode processing.

Watanabe *et al.* (118) analyzed the performance of two-dimensional constant-time correlation spectroscopy (CT-COSY) at 4.7 Tesla and was able to detect Gln and Glu, as well as other metabolites. Furthermore, Watanbe *et al.* demonstrated a CT-COSY spectrum (CT value of 110ms, 150 t1 increments) processed with Gaussian window functions revealed distinct diagonal peaks for protons on C4 of Glu and Gln (118). In this study data was acquired from the parieto-occipital region with a voxel size of 27ml. No numerical quantification or metabolite ratios were undertaken.

Recently, Gu *et al.* was able to determine concentrations of Glu and Gln in a phantom and in *in vivo* rat brains by fitting the one-dimensional CT-PRESS diagonal magnitude basis spectra to the measured spectrum (122). The one dimensional, effectively decoupled, magnitude spectra were extracted from the diagonal of two-dimensional CT-COSY spectra and fitted to suitably simulated basis sets. This method shows promise for human implementation, but was only tested in a phantom and rat brain at 3 Tesla, and has not yet been reported in human studies.

All the above 2D methods are still in development mode and require a high level of expertise from researchers to ensure reliable results. When mature, these methods are expected to produce more accurate results than their one dimensional counterparts for the majority, if not all, cerebral metabolites, including Glu and Gln. The current obvious drawback of these methods is the time taken to acquire the 2D data sets which is currently 15-25 minutes, unless ultra-fast techniques are adopted as described elsewhere (123). See Table 1 for a summary of quantification obtained from 2D methods.

3.3. 1D ^{13}C MRS Techniques

Carbon-13 (^{13}C) MRS is presently the only method that provides non-invasive measurements of neuroenergetics and neurotransmitter cycling in the human brain. ^{13}C MRS, combined with the administration of ^{13}C-labeled substrates, allows the for detection of ^{13}C incorporation from ^{13}C-labeled precursors into various carbon positions of metabolites, such as tricarboxylic acid cycle intermediates as well as the Glu-Gln and GABA-Gln cycles between neuronal and glial compartments (8). It allows for continuous, non-invasive monitoring of metabolic fluxes under different physiological or pathophysiological conditions. Furthermore, a wide spectral window (>200ppm), makes ^{13}C MRS ideal for obtaining semi-quantitative information about enriched substrates and their intermediates from within the brain in real-time.

The ^{13}C MRS acquisition consists of several different steps providing multiple means by which Glu can be measured. These include: choice of substrate (glucose, acetate, label position), method of delivery (oral, IV, glucose-clamped), data acquisition (direct detection, indirect detection), and method of analysis (dynamic difference spectroscopy, isotopomer analysis). Below is a description of each of the different methods. It is important to note that the natural abundance of ^{13}C is approximately 1.1% which implies that there is very little background signal of indigenous ^{13}C Glu, therefore, providing excellent contrast to noise

ratio of signals that arise from the incorporation of the ^{13}C label via the TCA cycle and subsequent transamination from alpha-ketoglutarate to the Glu-Gln cycle.

In *in vivo* ^{13}C MRS, glucose is labeled with an isotope of ^{13}C replacing one or more of the six carbons that make up the molecule. Depending on the choice of carbon, different parts of the Glu molecule will be labeled. C1 label of Glu resonates at 175.3ppm, C2 at 55.7ppm, C3 at 27.9ppm, C4 at 34.4ppm, and C5 at 182.0ppm (124). The position of the ^{13}C label has different implications for how Glu is detected and measured in post-processing of the ^{13}C data. For example, if the label is placed on the 1st carbon, the first turn of the TCA cycle will label the fourth carbon of Glu whereas if the label is placed on the 2nd carbon, Glu will be first labeled on the second carbon as shown in Figure 4. It is important to note that there can be several turns of the TCA cycle such that at the end of the first turn of the TCA cycle, the ^{13}C label will be on C2 and C3 of oxaloacetate which in turn labels C2, C3-Glu in the second turn as shown in Figure 4 and spectra shown in Figure 5. Thus, a time course of enrichment can be established allowing for the dynamic characterization of Glu neurotransmission.

While glucose has been shown to be almost entirely taken up and metabolized in the neuron, an alternative ^{13}C tracer is acetate, which has been shown to be preferentially taken up by astrocytes. This has the advantage of examining Glu metabolism in diseases of glial origin (125). When 1-^{13}C-acetate is administered, Glu is labeled at C5 which also implies that simultaneous administration of 1-^{13}C-glucose and 1-^{13}C-acetate can assess both neuronal and glial dysfunction simultaneously (126). Acetate is also useful for assessing Glu dysfunction in patients that cannot tolerate glucose infusions. The first human acetate studies were collected in epileptics that were being treated with a ketogenic diet whereby glucose exposure would result in seizures (125). The results of the study revealed that Glu metabolism was significantly reduced in these patients.

The substrates can also be delivered through a number of different means. The substrate is pyrogenically tested and then prepared by a pharmacy as a solution by which the concentration is dependent on the protocol and the weight of the patient. For example, an oral dosage requires a greater concentration of ^{13}C substrate whereas IV infusion requires a much lower concentration (127). Given the expense of ^{13}C glucose and the fact that not all of the labeled glucose is taken up into the brain, IV infusion is generally preferred. The IV infusion can be conducted with and without a glucose clamp. The advantage of the glucose clamp is that it provides steady-state concentrations of cerebral ^{13}C labeled glucose during the experiment such that TCA cycle rates and metabolic formation rates can be calculated and compared with animal studies and classic ^{13}C studies (128). However, glucose clamps require approximately four times the amount of ^{13}C-labelled glucose, the use of somatostatin (which is not FDA approved in children), an extended amount of time in the scanner of approximately 2 hours, as well as nursing support. An alternative utilizes pseudo or partial steady state concentrations of glucose, which doesn't allow for exact TCA cycle rates, but measures such as time-to-appearance and ratios of infusion at different time points can be utilized to explore Glu metabolism. This allows for a protocol that is clinically more feasible.

This then leads to the choice of data acquisition methods. ^{13}C MRS can be conducted using proton-decoupling in order to take advantage of the 2 to 3 times SNR gain through decoupling of the resonances and the nuclear Overhauser effect (129). The proton decoupling is achieved, on most systems, using the WALTZ-16 decoupling scheme (130) which is comprised of a 16-step decoupling super cycle using WALTZ ($90°_x$ $180°_x$ $270°_x$) pulses. Proton-decoupled ^{13}C data is acquired during the application of the WALTZ decoupling scheme. One of the drawbacks to this method is that the natural abundance

signal of lipid arising from the skull is collected which overlaps with the C4-Glu region of the ^{13}C spectrum. The lipid signal can be removed by subtracting baseline scans acquired prior to glucose infusion from the post-infusion data thus providing "dynamic difference spectroscopy" method of ^{13}C data analysis as shown in Figure 5. The difference spectroscopy approach is more applicable in the clinical environment and such has been primarily utilized by Brian Ross and colleagues to explore different human diseases as detailed below. In an effort to shorten the demands on scanner scheduling, methods have been developed to shorten the scan time. One method, the 'Snapshot' ^{13}C protocol consists of two short ^{13}C scan sessions, one at baseline (35 min acquisition) and the other two hours post infusion (20 min acquisition time) (131). More recently, Sailasuta *et al.* developed a similar protocol for acetate infusion, named "SAGA" (Swift Acetate Glial Assay) (132) which not only has the advantage of a reduced scan time (25.6 minutes due to acquisition only at 65 minutes post infusion) but also reduced power deposition by using a low power noise decoupling so that data can be acquired in the anterior lobe without the risk of SAR deposition to the eyeballs. It is important to note however the introduction of error if the subject is not placed in the same position at baseline and after infusion.

Alternatively, localized ^{13}C spectroscopy can be utilized to avoid errors that are related to region-of-interest repositioning before and after infusion. However, spatial localization for ^{13}C MRS is challenging given the low SNR as well as the large chemical shift dispersion of ^{13}C signals, the lack of spin-echo or stimulated echo sequences, and power absorption limits. The first sequence utilized three dimensional localization on the proton z magnetization combined with polarization transfer (133). Other polarization transfer methods can also be used, such as INEPT (insensitive nuclei enhanced by polarization transfer) with BIR-4 pulses (134). Outer volume suppression pulses, the use of adiabatic pulses such as with ISIS localization, as well as WALTZ-16 proton decoupling (2) are also methods of ^{13}C localization. The use of these methods yields the "isotopomer analysis" of the cerebral ^{13}C Glu. As most of the experiments associated with this methodology are conducted under glucose-clamp, TCA cycle rate (V_{TCA}) and rate of transamination between alpha-ketoglutarate and Glu (V_x) can be directly modeled and measured to provide quantitative assessments of glutamatergic neurotransmission (135). Finally, there are indirect detection methods whereby proton signal is observed and the heteronuclear coupling of ^{13}C signal is exploited. Given the large gyromagnetic ratio and natural abundance of proton signal, these methods provide much greater SNR and ease of localization. Methods such as single shot multiple quantum coherence spectroscopy and J-difference editing can be used for the indirect detection of ^{13}C signal in Glu as well as polarization transfer (136). Methods such as single-shot inversion recovery based non-echo (SIRENE) 2D localization methods can be used to detect Glu as well as metabolites with very short T1 and T2 such as glycogen (137). For details of these different methods, please see a recent thorough review by de Graaf *et al.* (8).

While ^{13}C MRS of brain Glu provides tremendous information about Glu metabolism, ^{13}C MRS studies are time-consuming, expensive, and technically challenging given the low SNR of the ^{13}C signal. One possible method of overcoming this problem would be the use of ^{13}C hyperpolarization, a recently developed method of increasing the polarization of molecules thus increasing overall SNR by several orders of magnitude. There have been some interesting studies that move towards this direction: Allouche-Arnon *et al*. have done this and observed the distribution of hyperpolarized glucose in a live rat (138). The metabolic products were not observed which is likely due to the short T1 relaxation time of glucose such that by the time it is metabolized, it is no longer polarized. One approach may be to hyperpolarize an intermediate metabolite within the TCA cycle such as succinate (139,140) or fumerate (141) however to date these methods have not been shown to result in hyperpolarized Glu. Finally, one could hyperpolarize Glu itself (142) which undergoes

transamination with alpha-ketoglutarate. The problem with this method is the blood-brain barrier which would prevent the rapid uptake of the hyperpolarized Glu to the brain. If the rapid decay of the hyperpolarized signal due to T1 and/or blood-brain barrier issues can be overcome, this method could show great promise in simplifying the current ^{13}C methods *in vivo*.

3.4. ^{13}C of Glu in Human Disease

While a number of studies have utilized the methods described above in animals and healthy controls, very few studies have been conducted in human disease. The vast majority of studies in human disease state have utilized the dynamic difference spectroscopy method (131). The first study to utilize this method was in chronic hepatic encephalopathy (CHE) (143) which presents a unique condition in which Glu-Gln interactions can be explored using ^{13}C MRS *in vivo*. ^{13}C MRS provides a direct window into the Glu-Gln cycle which is responsible for the removal of damaging ammonia in CHE. [1-^{13}C] glucose was infused into six patients and as expected, concentrations of Gln in the brain were found to be significantly increased. However, of greater interest, measures of the concentration of C4-Glu as well as fractional enrichment of C2- and C4-Glu were found to be half of that compared to healthy subjects, revealing striking Glu abnormalities in CHE. These results were confirmed in a follow-up study in which different grades of HE also showed corresponding reductions in cerebral Glu metabolism (143).

The effect of ammonia on the Glu-Gln cycle is only one mechanism of altering brain Glu levels. A number of other ^{13}C studies have explored the effect of disease on Glu metabolism whereby Glu dysfunction is a result of very different mechanisms. For example, patients with ornithine transcarbamylase deficiency, a rare inherited enzyme deficiency, also show reduced cerebral Glu metabolism however unlike CHE, Gln metabolism remained unchanged. This indicates a very different mechanism at the TCA cycle interface which in turn could be potentially targeted by pharmaceutical intervention. Other studies that have also shown reduced Glu metabolism include hypoxia (144) and epilepsy (126).

The role of Glu in Alzheimer's disease has also been explored in detail using ^{13}C MRS. The initial study in AD utilized [1-^{13}C] glucose in patients clinically diagnosed with AD as well as age-matched controls (41). The results of the study showed reduced Glu neurotransmission as measured by examining the time course of enrichment of Glu via the TCA cycle as well as relative enrichment of Glu to Gln. The time course measurements reflect the neuroenergetics of the brain and effectively measure TCA cycles rates. In AD patients, these rates were found to be reduced. The measure of C2-Glu and C2-Gln enrichment is of particular interest as it is reflective of Glu neurotransmission in itself. The ratio of Glu to Gln is indicative of the metabolic pool sizes of the two metabolites such that a change in the distribution of the metabolic load of neurons and astrocytes can be measured. For example, if the glial TCA cycle is operating faster, then an enrichment pattern with relatively increased Gln signal versus Glu signal would be expected. In this study, Glu/Gln ratios were found to be significantly decreased, reflective of decreased neurotransmission. More interestingly, when correlated with NAA measures as a surrogate marker for neuronal integrity, significant correlates were found with Glu/Gln ratios, further supporting the argument that this measure may be reflective of Glu neurotransmission in of itself. As NAA, or the number neurons decreased, Glu/Gln decreased, thus demonstrating that Glu neurotransmission may be decreased as a result in the reduction of the number of functioning brain cells. This study was followed up by an isotopomer analysis study by Boumezbeur *et al.* that compared Glu metabolism in healthy young adults and elderly adults (57). Their study not only confirmed the correlation between NAA and Glu metabolism but also utilized [2-^{13}C] acetate, the preferred fuel for astrocytes, and found a correlation

between Glu metabolism arising from the astrocyte and NAA decreases as well. Sailasuta *et al.* also found that using [1-^{13}C] acetate, the third turn of the TCA cycle, which produces bicarbonate, is significantly slower in AD patients when compared to controls (20).

Acetate is also the preferred ^{13}C tracer for the study of type 1 diabetes given the dangers of infusing glucose in those patients. Using isotopomer analysis, Mason *et al.* measured changes in Glu and Gln after the infusion of [2-^{13}C] acetate during hypoglycaemia (15). The results of their study showed a two- to three-fold increase in the labeling of C4-Glu and Gln as well as an increased uptake and utilization of acetate in the diabetic brain. One of the largest ^{13}C human studies also utilized ^{13}C acetate which was conducted in abstinent methamphetamine abusers by Sailasuta *et al.* (145). 21 subjects were examined using dynamic difference spectroscopy both in the posterior part of the brain using traditional proton-decoupled methods as well as in the frontal lobe using low RF power ^{13}C MRS (20). In this study glial TCA cycle rates were found to be severely reduced in drug abusers which in turn results in the accumulation of Glu in the brain, particularly in the frontal lobe as has been shown in proton studies in the same cohort of subjects (145).

In conclusion, ^{13}C MRS offers a unique window into the metabolism of brain Glu that goes far beyond the static measures of Glu found in conventional proton spectroscopy. The observation and characterization of the different parts of the TCA and Glu-Gln cycle via enrichment of specific carbons of Glu and Gln as well as the determination of neuronal and glial Glu function via glucose and acetate infusion, respectively, provides highly detailed information into Glu metabolism. This insight is not only valuable for the basic understanding of diseases but can also be potentially diagnostically important. Furthermore, identification of defects along the TCA and Glu-Gln pathway may yield specific targets for pharmaceutical interventions. Given the non-invasive nature of both the ^{13}C tracer and MR itself, ^{13}C MRS of Glu could also be used for therapeutic monitoring of those potential drug treatments.

4. Future prospects for Glu/Gln MRS studies in Humans

Over the past decade as our familiarity with the performance and interpretation of *in vivo* ^{1}H MRS has increased, there has been increased recognition of the significance of Glu and Gln in the human brain. Whilst early studies focused primarily on alterations in Glx, the advent of scanners operating at higher magnetic field strength, as well as the development of advanced spectral-editing techniques, have allowed for evaluation of Glu and Gln separately. This has allowed for investigation of the role of Glu and Gln in human disease. There is also increasing awareness in the role of neuroenergetics and glutamatergic neurotransmission in neurologic disorders and MRS examinations can provide direct non-invasive measurements of metabolic fluxes in the human brain. Accordingly, future ^{1}H MRS studies are likely to elucidate the role of glutamatergic abnormalities in neurologic conditions (e.g. neuro-degeneration, epilepsy, neuropsychiatry) and hold the possibility that individual measures of Glu and Gln may aid in refining diagnosis and developing novel and improved therapeutics that result in more personalized treatment regimens for individual patients than are currently available.

From the above survey of existing techniques for Glu/Gln quantitation, it is expected that ^{1}H 2D spectral methods, echo-planar spectroscopic imaging methods, as well as enriched ^{13}C MRS techniques at higher magnetic fields to play integral roles in future studies.

5. Conclusion

There is increasing interest in the role of Glu and Gln in human neurophysiology (e.g. neurotransmission, aging, pain, and perception), mental illness and disease processes (brain tumors, Alzheimer's disease, chronic hepatic encephalopathy). *In vivo* spectroscopy has the potential to non-invasively detect and monitor relevant metabolic changes, with one-dimensional and two-dimensional ^{1}H spectroscopy techniques being important tools to investigate and quantify changes to these important amino acids. Attractive features of these techniques include high inherent SNR, as well as absence of any exogenous material that needs to be infused in the body to perform measurements. However, speed, reproducibility and full brain coverage are essential factors that need to be improved for these techniques to be become commonplace in routine clinical imaging studies.

Challenges to ^{13}C Glu/Gln studies are numerous and many improvements are needed to reduce cost, improve technical capability on most human systems and reduce tissue heating. Once benefits become apparent, it's hoped that manufacturers will increase support for ^{13}C spectroscopy, and for heteronuclear capability, on most systems. Availability of high static magnetic fields and hyperpolarization techniques represent two major advances in the right direction.

The described methods in this article describe the currently available MRS methods and techniques to study Glu and Gln in the human brain. Spectroscopic methods, whether ^{1}H or ^{13}C, will continue to be integral in understanding the role of different brain metabolites in neuroenergetics and neurotransmission.

Acknowledgments

Support for S.R. from the School of Health Sciences at the University of Newcastle is acknowledged. A.L. would like to acknowledge support from the Department of Defense Psychological Health/Traumatic Brain Injury Research Program of the Office of the Congressionally Directed Medical Research Programs (W81XWH-10-1-0835), the National Institutes of Health / National Institute of Neurological Disorders and Stroke (R01 NS 078337), and the Center for Integration of Medicine (CIMIT) Innovation Grants.

Abbreviations

1D	one-dimensional
2D	two-dimensional
2DFT	two-dimensional Fourier transform
AD	Alzheimer's disease
ACC	anterior cingulate cortex
AP	anterior-posterior
ATP	adenosine triphosphate
BIR-4	B1-insensitive rotation type 4
CHE	chronic hepatic encephalopathy
Cho	Choline
COSY	correlation spectroscopy
C-PRESS	Carr-Purcell PRESS
Cr	Creatine

CRLB	Cramer–Rao Lower Bounds
CT-COSY	constant-time correlation spectroscopy
CV	coefficient of variation
EAAT	excitatory amino acid transporters
EPI	echo planar imaging
FID	free induction decay
FOV	field of view
GABA	γ-aminobutyric acid
GAMMA	general approach for magnetic resonance mathematical analysis
Gln	Glutamine
Glu	Glutamate
GluCEST	Glu **C**hemical **E**xchange **S**aturation **T**ransfer
Glx	Glutamine+Glutamate
GM	gray matter
GRAPPA	Generalized Autocalibrating Partially Parallel Acquisitions
HE	hepatic encephalopathy
GSH	Glutathione
INEPT	insensitive nuclei enhanced by polarization transfer
ISIS	image-selected *in vivo* spectroscopy
JPRESS	J-resolved spectroscopy
LASER	localization by adiabatic selective refocusing
LCModel	linear combination of model spectra
mI	myoinositol
mM	millimolar
MRS	magnetic resonance spectroscopy
MRSI	magnetic resonance spectroscopic imaging
ms	millisecond
MS	multiple sclerosis
NAA	N-acetylaspartate
NEX	number of excitations
PEPSI	Proton Echo-Planar Spectroscopic Imaging
ppm	parts per million
PRESS	Point resolved spectroscopy
ProFit	Prior-Knowledge Fitting
RF	radio frequency
SAGA	Swift Acetate Glial Assay

SAR	specific absorption rate
SENSE	Sensitivity Encoding
SNR	signal-to-noise ratio
STEAM	stimulated echo acquisition mode
T1	longitudinal relaxation
T2	transverse relaxation
tCho	total choline
TE	echo time
tCr	total creatine
TR	repetition time
WM	white matter

References

1. Govindaraju V, Young K, Maudsley AA. Proton NMR chemical shifts and coupling constants for brain metabolites. NMR Biomed. 2000; 13:129–153. [PubMed: 10861994]
2. Gruetter R, Novotny EJ, Boulware SD, Mason GF, Rothman DL, Shulman GI, Prichard JW, Shulman RG. Localized ^{13}C NMR spectroscopy in the human brain of amino acid labeling from d-[1-^{13}C]glucose. Journal of Neurochemistry. 1994; 63:1377–1385. [PubMed: 7931289]
3. Mason GF, Gruetter R, Rothman DL, Behar KL, Shulman RG, Novotny EJ. Simultaneous determination of the rates of the TCA cycle, glucose utilization,alph-aketoglutarate/Glutamate exchange, and glutamine synthesis in human brain by NMR. Journal of Cerebral Blood Flow and Metabolism. 1995; 15:12–25. [PubMed: 7798329]
4. Schousboe A. Role of astrocytes in the maintenance and modulation of glutamatergic and GABAergic neurotransmission. Neurochemical Research. 2003; 28:347–352. [PubMed: 12608708]
5. Schousboe A, Waagepetersen H. Role of astrocytes in glutamate homeostasis: Implications for excitotoxicity. Neurotoxicity Research. 2005; 8:221–225. [PubMed: 16371316]
6. Hertz L, Zielke HR. Astrocytic control of glutamatergic activity: astrocytes as stars of the show. Trends in Neurosciences. 2004; 27:735–743. [PubMed: 15541514]
7. Bak LK, Schousboe A, Waagepetersen HS. The glutamate/GABA-glutamine cycle: aspects of transport, neurotransmitter homeostasis and ammonia transfer. Journal of Neurochemistry. 2006; 98:641–653. [PubMed: 16787421]
8. de Graaf RA, Rothman DL, Behar KL. State of the art direct 13C and indirect 1H-[13C] NMR spectroscopy in vivo. A practical guide. NMR Biomed. 2011; 24:958–972. [PubMed: 21919099]
9. Sibson NR, Dhankhar A, Mason GF, Rothman DL, Behar KL, Shulman RG. Stoichiometric coupling of brain glucose metabolism and glutamatergic neuronal activity. Proceedings of the National Academy of Sciences of the United States of America. 1998; 95:316–321. [PubMed: 9419373]
10. Pellerin L, Magistretti P. Glutamate uptake into astrocytes stimulates aerobic glycolysis: A mechanism coupling neuronal activity to glucose utilization. Proceedings of the National Academy of Sciences of the United States of America. 1994; 91:10625–10629. [PubMed: 7938003]
11. Daikhin Y, Yudkoff M. Compartmentation of Brain Glutamate Metabolism in Neurons and Glia. Journal of Nutrition. 2000; 130:1026S–1031S. [PubMed: 10736375]
12. Novotny EJ, Fulbright RK, Pearl PL, Gibson KM, Rothman DL. Magnetic resonance spectroscopy of neurotransmitters in human brain. Annals of Neurology. 2003; 54:S25–S31. [PubMed: 12891651]
13. Petroff OAC. GABA and Glutamate in the Human Brain. The Neuroscientist. 2002; 8:562–573. [PubMed: 12467378]

14. Goudet C, Magnaghi V, Landry M, Nagy F, Gereau RW, Pin JP. Metabotropic receptors for glutamate and GABA in pain. Brain Res. Rev. 2009; 60:43–56. [PubMed: 19146876]
15. Mason GF, Krystal JH. MR spectroscopy: its potential role for drug development for the treatment of psychiatric diseases. NMR Biomed. 2006; 19:690–701. [PubMed: 16986118]
16. Yudkoff M, Daikhin Y, Melo TM, Nissim I, Sonnewald U, Nissim I. The ketogenic diet and brain metabolism of amino acids: Relationship to the anticonvulsant effect. Annual Review of Nutrition. 2007; 27:415–430.
17. Scott CJM, Szilagyi GM, Chavez S, Ganda A, Black SE. Applications of chemical shift imaging for AD. Current Medical Imaging Reviews. 2011; 7:88–95.
18. Brennan BP, Hudson JI, Jensen JE, McCarthy J, Roberts JL, Prescot AP, Cohen BM, Pope HG, Renshaw PF, Ongur D. Rapid enhancement of glutamatergic neurotransmission in bipolar depression following treatment with riluzole. Neuropsychopharmacology. 2010; 35:834–846. [PubMed: 19956089]
19. Yuksel C, Ongur D. Magnetic resonance spectroscopy studies of glutamate-related abnormalities in mood disorders. Biological Psychiatry. 2010; 68:785–794. [PubMed: 20728076]
20. Sailasuta N, Ernst T, Chang L. Regional variations and the effects of age and gender on glutamate concentrations in the human brain. Magnetic Resonance Imaging. 2008; 26:667–675. [PubMed: 17692491]
21. Pouwels PJW, Frahm J. Regional metabolite concentrations in human brain as determined by quantitative localized proton MRS. Magnetic Resonance in Medicine. 1998; 39:53–60. [PubMed: 9438437]
22. Novotny E, Ashwal S, Shevell M. Proton magnetic resonance spectroscopy: an emerging technology in pediatric neurology research. Pediatric Research. 1998; 44:1–10. [PubMed: 9667363]
23. Haga KK, Khor YP, Farrall A, Wardlaw JM. A systematic review of brain metabolite changes, measured with 1H magnetic resonance spectroscopy, in healthy aging. Neurobiology of Aging. 2009; 30:353–363. [PubMed: 17719145]
24. Yildiz-Yesiloglu A, Ankerst DP. Review of 1H magnetic resonance spectroscopy findings in major depressive disorder: a meta-analysis. Psychiatry Research: Neuroimaging. 2006; 147:1–25.
25. Petroff OAC, Errante LD, Rothman DL, Kim JH, Spencer DD. Glutamate–glutamine cycling in the epileptic human hippocampus. Epilepsia. 2002; 43:703–710. [PubMed: 12102672]
26. Cavus I, Kasoff WS, Cassaday MP, Jacob R, Gueorguieva R, Sherwin RS, Krystal JH, Spencer DD, Abi-Saab WM. Extracellular metabolites in the cortex and hippocampus of epileptic patients. Annals of Neurology. 2005; 57:226–235. [PubMed: 15668975]
27. Pan JW, Lane JB, Hetherington H, Percy AK. Rett Syndrome: 1H spectroscopic imaging at 4.1 tesla. Journal of Child Neurology. 1999; 14:524–528. [PubMed: 10456763]
28. Köstler H. Proton magnetic resonance spectroscopy in portal-systemic encephalopathy. Metabolic Brain Disease. 1998; 13:291–301. [PubMed: 10206821]
29. Có'rdoba J, Sanpedro F, Alonso J, Rovira A. ^{1}H magnetic resonance in the study of hepatic encephalopathy in humans. Metabolic Brain Disease. 2002; 17:415–429. [PubMed: 12602517]
30. Rovira A, Alonso J, Cordoba J. MR imaging findings in hepatic encephalopathy. AJNR: American Journal of Neuroradiology. 2008; 29:1612–1621. [PubMed: 18583413]
31. Hazany S, Hesselink JR, Healy J, Imbesi S. Utilization of glutamate/creatine ratios for proton spectroscopic diagnosis of meningiomas. Neuroradiology. 2007; 49:121–127. [PubMed: 17086406]
32. Horska A, Barker PB. Imaging of brain tumors: MR spectroscopy and metabolic imaging. Neuroimaging Clinics of North America. 2010; 20:293–310. [PubMed: 20708548]
33. Tate AR, Underwood J, Acosta DM, Julia-Sape M, Majos C, Moreno-Torres A, Howe FA, van der Graaf M, Lefournier V, Murphy MM, Loosemore A, Ladroue C, Wesseling P, Bosson JL, Cabanas ME, Simonetti AW, Gajewicz W, Calvar J, Capdevila A, Wilkins PR, Bell BA, Remy C, Heerschap A, Watson D, Griffiths JR, Arus C. Development of a decision support system for diagnosis and grading of brain tumours using in vivo magnetic resonance single voxel spectra. NMR Biomed. 2006; 19:411–434. [PubMed: 16763971]

34. Cianfoni A, Niku S, Imbesi SG. Metabolite findings in tumefactive demyelinating lesions utilizing short echo time proton magnetic resonance spectroscopy. AJNR: American Journal of Neuroradiology. 2007; 28:272–277. [PubMed: 17296993]
35. De Witte P. Imbalance between neuroexcitatory and neuroinhibitory amino acids causes craving for ethanol. Addictive Behaviors. 2004; 29:1325–1339. [PubMed: 15345268]
36. Licata SC, Renshaw PF. Neurochemistry of drug action: insights from proton magnetic resonance spectroscopic imaging and their relevance to addiction. Annals of the New York Academy of Sciences. 2010; 1187:148–171. [PubMed: 20201852]
37. Harrison PJ, Weinberger DR. Schizophrenia genes, gene expression, and neuropathology: on the matter of their convergence. Molecular Psychiatry. 2004; 10:40–68. [PubMed: 15263907]
38. Theberge J, Al-Semaan Y, Williamson PC, Menon RS, Neufeld RW, Rajakumar N, Schaefer B, Densmore M, Drost DJ. Glutamate and glutamine in the anterior cingulate and thalamus of medicated patients with chronic schizophrenia and healthy comparison subjects measured with 4.0-T proton MRS. American Journal of Psychiatry. 2003; 160:2231–2233. [PubMed: 14638596]
39. Shutter L, Tong KA, Holshouser BA. Proton MRS in acute traumatic brain injury: role for glutamate/glutamine and choline for outcome prediction. Journal of Neurotrauma. 2004; 21:1693–1705. [PubMed: 15684761]
40. Ashwal S, Holshouser B, Tong K, Serna T, Osterdock R, Gross M, Kido D. Proton MR spectroscopy detected glutamate/glutamine is increased in children with traumatic brain injury. Journal of Neurotrauma. 2004; 21:1539–1552. [PubMed: 15684647]
41. Lin AP, Shic F, Enriquez C, Ross BD. Reduced glutamate neurotransmission in patients with Alzheimer's disease–an in vivo ^{13}C magnetic resonance spectroscopy study. Magnetic Resonance Materials in Physics, Biology and Medicine. 2003; 16:29–42.
42. Martin WRW. MR spectroscopy in neurodegenerative disease. Molecular Imaging and Biology. 2007; 9:196–203. [PubMed: 17279431]
43. Kreis R, Hofmann L, Kuhlmann B, Boesch C, Bossi E, Huppi PS. Brain metabolite composition during early human brain development as measured by quantitative in vivo 1H magnetic resonance spectroscopy. Magnetic Resonance in Medicine. 2002; 48:949–958. [PubMed: 12465103]
44. Kreis R, Pfenninger J, Herschkowitz N, Boesch C. In vivo proton magnetic resonance spectroscopy in a case of Reye's syndrome. Intensive Care Medicine. 1995; 21:266–269. [PubMed: 7790619]
45. Gropman AL, Summar M, Leonard JV. Neurological implications of urea cycle disorders. J. Inherit. Metab. Dis. 2007; 30:865–879. [PubMed: 18038189]
46. Kreis R, Ross BD, Farrow NA, Ackerman Z. Metabolic disorders of the brain in chronic hepatic encephalopathy detected with H-1 MR spectroscopy. Radiology. 1992; 182:19–27. [PubMed: 1345760]
47. Thomas MA, Huda A, Guze B, Curran J, Bugbee M, Fairbanks L, Ke Y, Oshiro T, Martin P, Fawzy F. Cerebral 1H MR spectroscopy and neuropsychologic status of patients with hepatic encephalopathy. American Journal of Roentgenology. 1998; 171:1123–1130. [PubMed: 9763008]
48. Ross BD, Jacobson S, Villamil F, Korula J, Kreis R, Ernst T, Shonk T, Moats RA. Subclinical hepatic encephalopathy: proton MR spectroscopic abnormalities. Radiology. 1994; 193:457–463. [PubMed: 7972763]
49. Lin A, Ross BD, Harris K, Wong W. Efficacy of proton magnetic resonance spectroscopy in neurological diagnosis and neurotherapeutic decision making. NeuroRx. 2005; 2:197–214. [PubMed: 15897945]
50. Rijpkema M, Schuuring J, van der Meulen Y, van der Graaf M, Bernsen H, Boerman R, van der Kogel A, Heerschap A. Characterization of oligodendrogliomas using short echo time 1H MR spectroscopic imaging. NMR Biomed. 2003; 16:12–18. [PubMed: 12577293]
51. Chawla S, Oleaga L, Wang S, Krejza J, Wolf RL, Woo JH, O'Rourke DM, Judy KD, Grady MS, Melhem ER, Poptani H. Role of proton magnetic resonance spectroscopy in differentiating oligodendrogliomas from astrocytomas. Journal of Neuroimaging. 2010; 20:3–8. [PubMed: 19021846]

52. Chawla S, Wang S, Wolf RL, Woo JH, Wang J, O'Rourke DM, Judy KD, Grady MS, Melhem ER, Poptani H. Arterial spin-labeling and MR spectroscopy in the differentiation of gliomas. AJNR: American Journal of Neuroradiology. 2007; 28:1683–1689. [PubMed: 17893221]
53. Majos C, Julia-Sape M, Alonso J, Serrallonga M, Aguilera C, Acebes JJ, Arus C, Gili J. Brain tumor classification by proton MR spectroscopy: comparison of diagnostic accuracy at short and long TE. AJNR: American Journal of Neuroradiology. 2004; 25:1696–1704. [PubMed: 15569733]
54. Pan JW, Williamson A, Cavus I, Hetherington HP, Zaveri H, Petroff OAC, Spencer DD. Neurometabolism in human epilepsy. Epilepsia. 2008; 49:31–41. [PubMed: 18304254]
55. Lin MT, Beal MF. Mitochondrial dysfunction and oxidative stress in neurodegenerative diseases. Nature. 2006; 443:787–795. [PubMed: 17051205]
56. Zhou YX, Kierans A, Kenul D, Ge YL, Rath J, Reaume J, Grossman RI, Lui YW. Mild Traumatic Brain Injury: Longitudinal Regional Brain Volume Changes. Radiology. 2013; 267:880–890. [PubMed: 23481161]
57. Boumezbeur F, Mason GF, de Graaf RA, Behar KL, Cline GW, Shulman GI, Rothman DL, Petersen KF. Altered brain mitochondrial metabolism in healthy aging as assessed by in vivo magnetic resonance spectroscopy. Journal of Cerebral Blood Flow and Metabolism. 2009; 30:211–221. [PubMed: 19794401]
58. Prost RW, Mark L, Mewissen M, Li SJ. Detection of glutamate/glutamine resonances by H-1 magnetic resonance spectroscopy at 0.5 Tesla. Magnetic Resonance in Medicine. 1997; 37:615–618. [PubMed: 9094085]
59. Bolan PJ, DelaBarre L, Baker EH, Merkle H, Everson LI, Yee D, Garwood M. Eliminating spurious lipid sidebands in 1H MRS of breast lesions. Magnetic Resonance in Medicine. 2002; 48:215–222. [PubMed: 12210929]
60. Dreher W, Leibfritz D. On the use of 2-Dimensional-J NMR measurements for in vivo proton MRS-measurement of homonuclear decoupled spectra without the need for short echo times. Magnetic Resonance in Medicine. 1995; 34:331–337. [PubMed: 7500871]
61. Hurd R, Sailasuta N, Srinivasan R, Vigneron DB, Pelletier D, Nelson SJ. Measurement of brain glutamate using TE-averaged PRESS at 3T. Magnetic Resonance in Medicine. 2004; 51:435–440. [PubMed: 15004781]
62. Smith SA, Levante TO, Meier BH, Ernst RR. Computer-simulations in magnetic-resonance - an object-oriented programming approach. Journal of Magnetic Resonance Series A. 1994; 106:75–105.
63. Srinivasan R, Cunningham C, Chen A, Vigneron D, Hurd R, Nelson S, Pelletier D. TE-averaged two-dimensional proton spectroscopic imaging of glutamate at 3 T. Neuroimage. 2006; 30:1171–1178. [PubMed: 16431138]
64. Perry TL, Berry K, Hansen S, Diamond S, Mok C. Regional distribution of amino acids in human brain obtained at autopsy. Neurchemistry. 1971; 18:513–519.
65. Lavoie J, Giguere JF, Layrargues GP, Butterworth RF. Amino acid changes in autopsied brain tissue from cirrhotic patients with hepatic encephalopathy. J. Neurochem. 1987; 49:692–697. [PubMed: 2886551]
66. Schubert F, Gallinat J, Seifert F, Rinneberg H. Glutamate concentrations in human brain using single voxel proton magnetic resonance spectroscopy at 3 Tesla. Neuroimage. 2004; 21:1762–1771. [PubMed: 15050596]
67. Jang DP, Lee JM, Lee E, Park S, Kim JJ, Namkoong K, Yoon KJ, Kim IY, Kim SI. Interindividual reproducibility of glutamate quantification using 1.5-T proton magnetic resonance spectroscopy. Magnetic Resonance in Medicine. 2005; 53:708–712. [PubMed: 15723390]
68. Provencher SW. Automatic quantitation of localized in vivo 1H spectra with LCModel. NMR Biomed. 2001; 14:260–264. [PubMed: 11410943]
69. Mullins PG, Chen H, Xu J, Caprihan A, Gasparovic C. Comparative reliability of proton spectroscopy techniques designed to improve detection of J-coupled metabolites. Magnetic Resonance in Medicine. 2008; 60:964–969. [PubMed: 18816817]
70. Yang SL, Hu JN, Kou ZF, Yang YH. Spectral simplification for resolved glutamate and glutamine measurement using a standard STEAM sequence with optimized timing parameters at 3, 4, 4.7, 7, and 9.4 T. Magnetic Resonance in Medicine. 2008; 59:236–244. [PubMed: 18228589]

71. Forsen S, Hoffman RA. Study of moderately rapid chemical exchange reactions by means of nuclear magnetic double resonance. J. Chem. Phys. 1963; 39:2892–2901.
72. Cai K, Haris M, Singh A, Kogan F, Greenberg JH, Hariharan H, Detre JA, Reddy R. Magnetic resonance imaging of glutamate. Nature Medicine. 2012; 18:302–306.
73. Zhou J, Zijl PCMv. Chemical exchange saturation transfer imaging and spectroscopy. Progress in Nuclear Magnetic Resonance Spectroscopy. 2006; 48:109–136.
74. Wijtenburg SA, Knight-Scott J. Very short echo time improves the precision of glutamate detection at 3T in 1H magnetic resonance spectroscopy. Journal of Magnetic Resonance Imaging. 2011; 34:645–652. [PubMed: 21761460]
75. Ramadan S. Phase-Rotation in In-vivo Localised Spectroscopy. Concepts in Magnetic Resonance. 2007; 30:147–153.
76. Hennig J. The application of phase rotation for localized in vivo proton spectroscopy with short echo times. Journal of Magnetic Resonance. 1992; 96:40–49.
77. Mekle R, Mlynarik V, Gambarota G, Hergt M, Krueger G, Gruetter R. MR Spectroscopy of the Human Brain With Enhanced Singla Intensity at Ultrashort Echo Times on a Clinical Platform at 3T and 7T. Magnetic Resonance in Medicine. 2009; 61:1279–1285. [PubMed: 19319893]
78. Ordidge RJ, Connelly A, Lohman JAB. Image-selected invivo spectroscopy (ISIS) - a new technique for spatially selective NMR-spectroscopy. Journal of Magnetic Resonance. 1986; 66:283–294.
79. Kirov II, Tal A, Babb JS, Lui YW, Grossman RI, Gonen O. Diffuse axonal injury in mild traumatic brain injury: a 3D multivoxel proton MR spectroscopy study. Journal of Neurology. 2013; 260:242–252. [PubMed: 22886061]
80. Garwood M, DelaBarre L. The return of the frequency sweep: designing adiabatic pulses for contemporary NMR. Journal of Magnetic Resonance. 2001; 153
81. Kassem MNE, Bartha R. Quantitative proton short-echo-time LASER spectroscopy of normal human white matter and hippocampus at 4 Tesla incorporating macromolecule subtraction. Magnetic Resonance in Medicine. 2003; 49:918–927. [PubMed: 12704775]
82. Tkac I, Gruetter R. Methodology of 1H NMR spectrosocopy of human brain at very high magnetic fields. Applied Magnetic Resonance. 2005; 29:139–157. [PubMed: 20179773]
83. Tkac I, Andersen P, Adriany G, Merkle H, Ugurbil K, Gruetter R. In Vivo 1H NMR spectroscopy of the human brain at 7 T. Magnetic Resonance in Medicine. 2001; 46:451–456. [PubMed: 11550235]
84. Mangia S, Tkac I, Gruetter R, Van de Moortele PF, Maraviglia B, Ugurbil K. Sustained neuronal activation raises oxidative metabolism to a new steady-state level: evidence from H-1 NMR spectroscopy in the human visual cortex. Journal of Cerebral Blood Flow and Metabolism. 2007; 27:1055–1063. [PubMed: 17033694]
85. Schaller B, Mekle R, Xin LJ, Kunz N, Gruetter R. Net increase of lactate and glutamate concentration in activated human visual cortex detected with magnetic resonance spectroscopy at 7 tesla. Journal of Neuroscience Research. 2013; 91:1076–1083. [PubMed: 23378234]
86. Emir UE, Auerbach EJ, Van De Moortele PF, Marjanska M, Ugurbil K, Terpstra M, Tkac I, Oz G. Regional neurochemical profiles in the human brain measured by 1H MRS at 7 T using local B1 shimming. NMR Biomed. 2012; 25:152–160. [PubMed: 21766380]
87. Henning A, Fuchs A, Murdoch JB, Boesiger P. Slice-selective FID acquisition, localized by outer volume suppression (FIDLOVS) for H-1-MRSI of the human brain at 7 T with minimal signal loss. NMR Biomed. 2009; 22:683–696. [PubMed: 19259944]
88. Rothman DL, Behar KL, Hetherington HP, Shulman RG. Homonuclear H-1 double-resonance difference spectroscopy of the rat-brain invivo. Proceedings of the National Academy of Sciences of the United States of America-Biological Sciences. 1984; 81:6330–6334.
89. Mescher M, Merkle H, Kirsch J, Garwood M, Gruetter R. Simultaneous in vivo spectral editing and water suppression. NMR Biomed. 1998; 11:266–272. [PubMed: 9802468]
90. Waddell KW, Zanjanipour P, Pradhan S, Xu L, Welch EB, Joers JM, Martin PR, Avison MJ, Gore JC. Anterior cingulate and cerebellar GABA and Glu correlations measured by (1)H J-difference spectroscopy. Magnetic Resonance Imaging. 2011; 29:19–24. [PubMed: 20884148]

91. Lee HK, Yaman A, Nalcioglu O. Homonuclear J-refocused spectral editing technique for quantification of glutamine and glutamate by H-1-NMR spectroscopy. Magnetic Resonance in Medicine. 1995; 34:253–259. [PubMed: 7476085]
92. Snyder J, Thompson RB, Wilman AH. Difference spectroscopy using PRESS asymmetry: application to glutamate, glutamine, and myo-inositol. NMR Biomed. 2010; 23:41–47. [PubMed: 19688783]
93. Gambarota G, van der Graaf M, Klomp D, Mulkern RV, Heerschap A. Echo-time independent signal modulations using PRESS sequences: A new approach to spectral editing of strongly coupled AB spin systems. Journal of Magnetic Resonance. 2005; 177:299–306. [PubMed: 16169267]
94. Snyder J, Wilman A. Field strength dependence of PRESS timings for simultaneous detection of glutamate and glutamine from 1.5 to 7 T. Journal of Magnetic Resonance. 2010; 203:66–72. [PubMed: 20031459]
95. Hennig J, Thiel T, Speck O. Improved sensitivity to overlapping multiplet signals in in vivo proton spectroscopy using a multiecho volume selective (CPRESS) experiment. Magnetic Resonance in Medicine. 1997; 37:816–820. [PubMed: 9178230]
96. Mayer, D.; Spielman, DM. Detection of glutamate in the human brain at 3 Tesla using optimized CT-PRESS. Proceedings of the International Society of Magnetic Resonance in Medicine; Honolulu. 2002; p. 785
97. Hancu I. Optimized glutamate detection at 3T. Journal of Magnetic Resonance Imaging. 2009; 30:1155–1162. [PubMed: 19856449]
98. Choi C, Coupland NJ, Bhardwaj PP, Malykhin N, Gheorghiu D, Allen PS. Measurement of brain glutamate and glutamine by spectrally-selective refocusing at 3 tesla. Magnetic Resonance in Medicine. 2006; 55:997–1005. [PubMed: 16598736]
99. Posse S, Tedeschi G, Risinger R, Ogg R, Lebihan D. High-speed H-1 spectroscopic imaging in human brain by echo-planar spatial-spectral encoding. Magnetic Resonance in Medicine. 1995; 33:34–40. [PubMed: 7891533]
100. Posse S, Otazo R, Caprihan A, Bustillo J, Chen HJ, Henry PG, Marjanska M, GasparoviC C, Zuo C, Magnotta V, Mueller B, Mullins P, Renshaw P, Ugurbil K, Lim KO, Alger JR. Proton echo-planar spectroscopic imaging of J-coupled resonances in human brain at 3 and 4 Tesla. Magnetic Resonance in Medicine. 2007; 58:236–244. [PubMed: 17610279]
101. Otazo R, Tsai SY, Lin FH, Posse S. Accelerated Short-TE 3D proton echo-planar spectroscopic imaging using 2D-SENSE with a 32-channel array coil. Magnetic Resonance in Medicine. 2007; 58:1107–1116. [PubMed: 17968995]
102. Lin FH, Tsai SY, Otazo R, Caprihan A, Wald LL, Belliveau JW, Posse S. Sensitivity-encoded (SENSE) proton echo-planar spectroscopic imaging (PEPSI) in the human brain. Magnetic Resonance in Medicine. 2007; 57:249–257. [PubMed: 17260356]
103. Tsai SY, Otazo R, Posse S, Lin YR, Chung HW, Wald LL, Wiggins GC, Lin FH. Accelerated proton echo planar spectroscopic Imaging (PEPSI) using GRAPPA with a 32-channel phased-array coil. Magnetic Resonance in Medicine. 2008; 59:989–998. [PubMed: 18429025]
104. Thompson RB, Allen PS. A new multiple quantum filter design procedure for use on strongly coupled spin systems found In Vivo: its application to glutamate. Magnetic Resonance in Medicine. 1998; 39:762–771. [PubMed: 9581608]
105. Pan JW, Mason GF, Pohost GM, Hetherington HP. Spectroscopic imaging of human brain glutamate by water-suppressed J-refocused coherence transfer at 4.1 T. Magnetic Resonance in Medicine. 1996; 36:7–12. [PubMed: 8795013]
106. Provencher SW. Estimation of metabolite concentrations from localized in vivo proton NMR spectra. Magnetic Resonance in Medicine. 1993; 30:672–679. [PubMed: 8139448]
107. Gussew A, Rzanny R, Erdtel M, Scholle HC, Kaiser WA, Mentzel HJ, Reichenbach JR. Time-resolved functional H-1 MR spectroscopic detection of glutamate concentration changes in the brain during acute heat pain stimulation. Neuroimage. 2010; 49:1895–1902. [PubMed: 19761852]
108. Wijnen JR, van Asten JJA, Klomp DWJ, Sjobakk TE, Gribbestad IS, Scheenen TWJ, Heerschap A. Short echo time H-1 MRSI of the human brain at 3T with adiabatic slice-selective refocusing

pulses; reproducibility and variance in a dual center setting. Journal of Magnetic Resonance Imaging. 2010; 31:61–70. [PubMed: 20027568]

109. Naressi A, Couturier C, Devos JM, Janssen M, Mangeat C, de Beer R, Graveron-Demilly D. Java-based graphical user interface for the MRUI quantitation package. Magnetic Resonance Materials in Physics, Biology and Medicine. 2001; 12:141–152.
110. Aue WP, Bartholdi E, Ernst RR. Two-dimensional spectroscopy. Application to nuclear magnetic resonance. Journal of Chemical Physics. 1976; 64:2229–2246.
111. Aue WP, Karhan J, Ernst RR. HOMONUCLEAR BROAD-BAND DECOUPLING AND 2-DIMENSIONAL J-RESOLVED NMR-SPECTROSCOPY. Journal of Chemical Physics. 1976; 64:4226–4227.
112. Schulte RF, Boesiger P. ProFit: two-dimensional prior-knowledge fitting of *J*-resolved spectra. NMR Biomed. 2006; 19:255–263. [PubMed: 16541464]
113. Thomas MA, Yue K, Binesh N, Davanzo P, Kumar A, Siegel B, Frye M, Curran J, Lufkin R, Martin P, Guze B. Localized two-dimensional shift correlated MR spectroscopy of human brain. Magnetic Resonance in Medicine. 2001; 46:58–67. [PubMed: 11443711]
114. Thomas MA, Hattori N, Umeda M, Sawada T, Naruse S. Evaluation of two-dimensional L-COSY and JPRESS using a 3T MRI scanner: from phantoms to human brain in vivo. NMR Biomed. 2003; 16:245–251. [PubMed: 14648883]
115. Frias-Martinez, E.; Rajakumar, N.; Liu, X.; Singhal, A.; Banakar, S.; Lipnick, S.; Verma, G.; Ramadan, S.; Kumar, A.; Thomas, MA. ProFit-based Quantitation of Cerebral Metabolites using 2D L-COSY at 3T. proceedings of the Internation Society of Magnetic Resonance in Medicine; Toronto, Canada. 2008; p. 691
116. Ramadan S, Mountford C. Adiabatic Localized Correlation Spectroscopy (AL-COSY) – Application in Muscle and Brain. Journal of Magnetic Resonance Imaging. 2011; 33:1447–1455. [PubMed: 21591015]
117. Andronesi OC, Ramadan S, Mountford CE, Sorensen AG. Low-power adiabatic sequences for in vivo localized two-dimensional chemical shift correlated MR spectroscopy. Magnetic Resonance in Medicine. 2010; 64:1542–1556. [PubMed: 20890988]
118. Watanabe H, Takaya N, Mitsumori F. Simultaneous observation of glutamate, γ-aminobutyric acid, and glutamine in human brain at 4.7 T using localized two-dimensional constant-time correlation spectroscopy. NMR Biomed. 2008; 21:518–526. [PubMed: 18351694]
119. Jensen JE, Licata SC, Ongur D, Friedman SD, Prescot AP, Henry ME, Renshaw PF. Quantification of J-resolved proton spectra in two-dimensions with LCModel using GAMMA-simulated basis sets at 4 Tesla. NMR Biomed. 2009; 22:762–769. [PubMed: 19388001]
120. Chong DGQ, Kreis R, Bolliger CS, Boesch C, Slotboom J. Two-dimensional linear-combination model fitting of magnetic resonance spectra to define the macromolecule baseline using FiTAID, a Fitting Tool for Arrays of Interrelated Datasets. Magnetic Resonance Materials in Physics Biology and Medicine. 2011; 24:147–164.
121. Gonenc A, Govind V, Sheriff S, Maudsley AA. Comparison of Spectral Fitting Methods for Overlapping J-Coupled Metabolite Resonances. Magnetic Resonance in Medicine. 2010; 64:623–628. [PubMed: 20597119]
122. Gu M, Zahr NM, Spielman DM, Sullivan EV, Pfefferbaum A, Mayer D. Quantification of glutamate and glutamine using constant-time point-resolved spectroscopy at 3 T. NMR Biomed. 2013; 26:164–172. [PubMed: 22761057]
123. Giraudeau P, Massou S, Robin Y, Cahoreau E, Portais JC, Akoka S. Ultrafast Quantitative 2D NMR: An Efficient Tool for the Measurement of Specific Isotopic Enrichments in Complex Biological Mixtures. Analytical Chemistry. 2011; 83:3112–3119. [PubMed: 21417426]
124. Bluml S, Hwang JH, Moreno A, Ross BD. Novel peak assignments of in vivo (13)C MRS in human brain at 1.5 T. Journal of Magnetic Resonance. 2000; 143:292–298. [PubMed: 10729255]
125. Bluml S, Moreno-Torres A, Shic F, Nguy CH, Ross BD. Tricarboxylic acid cycle of glia in the in vivo human brain. NMR Biomed. 2002; 15:1–5. [PubMed: 11840547]
126. Shic F, Ross B. Automated data processing of [1H-decoupled] 13C MR spectra acquired from human brain in vivo. Journal of Magnetic Resonance. 2003; 162:259–268. [PubMed: 12810010]

127. Moreno A, Bluml S, Hwang JH, Ross BD. Alternative 1-(13)C glucose infusion protocols for clinical (13)C MRS examinations of the brain. Magnetic Resonance in Medicine. 2001; 46:39–48. [PubMed: 11443709]
128. Rothman DL, De Feyter HM, de Graaf RA, Mason GF, Behar KL. (13)C MRS studies of neuroenergetics and neurotransmitter cycling in humans. NMR Biomed. 2011; 24:943–957. [PubMed: 21882281]
129. de Graaf, RA. In vivo NMR spectroscopy: principles and techniques. John Wiley and Sons Inc; Chichester; New York: 2007. p. 118-119.
130. Shaka AJ, Keeler J, Frenkiel T, Freeman R. An improved sequence for broadband decoupling: WALTZ-16. Journal of Magnetic Resonance. 1983; 52:335–338.
131. Ross B, Lin A, Harris K, Bhattacharya P, Schweinsburg B. Clinical experience with C-13 MRS in vivo. NMR Biomed. 2003; 16:358–369. [PubMed: 14679500]
132. Sailasuta N, Tran TT, Harris KC, Ross BD. Swift Acetate Glial Assay (SAGA): an accelerated human 13C MRS brain exam for clinical diagnostic use. Journal of Magnetic Resonance. 2010; 207:352–355. [PubMed: 20934362]
133. Gruetter R, Adriany G, Merkle H, Andersen PM. Broadband decoupled, 1H-localized 13C MRS of the human brain at 4 Tesla. Magn Reson Med. 1996; 36:659–664. [PubMed: 8916015]
134. Shen J, Petersen KF, Behar KL, Brown P, Nixon TW, Mason GF, Petroff OA, Shulman GI, Shulman RG, Rothman DL. Determination of the rate of the glutamate/glutamine cycle in the human brain by in vivo 13C NMR. Proceedings of the National Academy of Sciences of the United States of America. 1999; 96:8235–8240. [PubMed: 10393978]
135. Gruetter R, Seaquist ER, Kim S, Ugurbil K. Localized in vivo C-13-NMR of glutamate metabolism in the human brain: Initial results at 4 Tesla. Developmental neuroscience. 1998; 20:380–388. [PubMed: 9778575]
136. Xu S, Yang J, Shen J. Inverse polarization transfer for detecting in vivo 13C magnetization transfer effect of specific enzyme reactions in 1H spectra. Magnetic Resonance Imaging. 2008; 26:413–419. [PubMed: 18063339]
137. Choi IY, Tkac I, Gruetter R. Single-shot, three-dimensional “non-echo” localization method for in vivo NMR spectroscopy. Magn Reson Med. 2000; 44:387–394. [PubMed: 10975890]
138. Allouche-Arnon H, Wade T, Waldner LF, Miller VN, Gomori JM, Katz-Brull R, McKenzie CA. In vivo magnetic resonance imaging of glucose - initial experience. Contrast Media Mol Imaging. 2013; 8:72–82. [PubMed: 23109395]
139. Zacharias NM, Chan HR, Sailasuta N, Ross BD, Bhattacharya P. Real-time molecular imaging of tricarboxylic acid cycle metabolism in vivo by hyperpolarized 1-^{13}C diethyl succinate. Journal of the American Chemical Society. 2012; 134:934–943. [PubMed: 22146049]
140. Bhattacharya P, Chekmenev EY, Perman WH, Harris KC, Lin AP, Norton VA, Tan CT, Ross BD, Weitekamp DP. Towards hyperpolarized ^{13}C-succinate imaging of brain cancer. Journal of Magnetic Resonance. 2007; 186:150–155. [PubMed: 17303454]
141. Gallagher FA, Kettunen MI, Hu DE, Jensen PR, Zandt RI, Karlsson M, Gisselsson A, Nelson SK, Witney TH, Bohndiek SE, Hansson G, Peitersen T, Lerche MH, Brindle KM. Production of hyperpolarized [1,4-^{13}C2]malate from [1,4-^{13}C2]fumarate is a marker of cell necrosis and treatment response in tumors. Proceedings of the National Academy of Sciences of the United States of America. 2009; 106:19801–19806. [PubMed: 19903889]
142. Gallagher FA, Kettunen MI, Day SE, Hu DE, Karlsson M, Gisselsson A, Lerche MH, Brindle KM. Detection of tumor glutamate metabolism in vivo using ^{13}C magnetic resonance spectroscopy and hyperpolarized [1-^{13}C]glutamate. Magnetic Resonance in Medicine. 2011; 66:18–23. [PubMed: 21695718]
143. Bluml S, Moreno-Torres A, Ross BD. [1-^{13}C]glucose MRS in chronic hepatic encephalopathy in man. Magnetic Resonance in Medicine. 2001; 45:981–993. [PubMed: 11378875]
144. Bluml S, Moreno A, Hwang JH, Ross BD. 1-^{13}C glucose magnetic resonance spectroscopy of pediatric and adult brain disorders. NMR Biomed. 2001; 14:19–32. [PubMed: 11252037]
145. Sailasuta N, Abulseoud O, Harris KC, Ross BD. Glial dysfunction in abstinent methamphetamine abusers. J Cereb Blood Flow Metab. 2010; 30:950–960. [PubMed: 20040926]

146. Frias-Martinez, E.; Rajakumar, N.; Ramadan, S.; Banakar, S.; Liu, X.; Singhal, A.; Thomas, MA. A Pilot Comparison of 2D and 1D MR Spectroscopic Quantitation of Metabolites in Healthy Human Brain at 3T. proceedings of the Internation Society of Magnetic Resonance in Medicine; Toronto, Canada. 2008; p. 1603

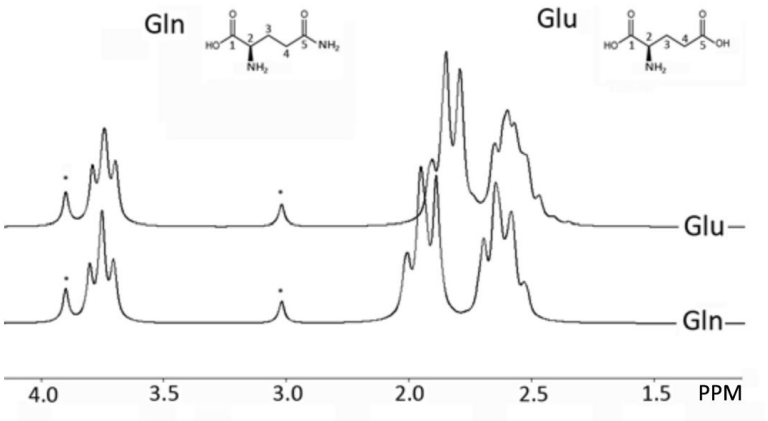

Figure 1.

Simulated 1D proton spectra of Glu and Gln with 5% Cr (peaks with *) at 3 Tesla. Notice the striking similarity of Glu and Gln structure and as a consequence, the spectral profile. A line broadening of 10 Hz was applied to spectra. Chemical shifts and scalar J-coupling were obtained from (1).

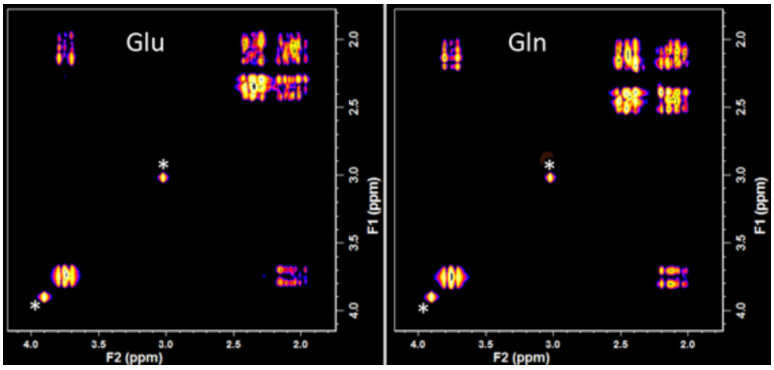

Figure 2.

Simulated 2D COSY proton spectra of Glu and Gln with 5% Cr (peaks with *, at 3.02 and 3.92ppm) at 3 Tesla. Notice the striking similarity of Glu and Gln spectral profiles. Spectra were simulated with 512 points in F2 and 200 points in F1 using a non-localized gradient COSY sequence (90° t1 G 90° G Acquire, G: gradient pulse), with 1.62ms increment, spectral width of 5ppm in both dimensions. Processing was performed by zero filling to 1024 points in both dimensions and weighting F2 and F1 dimensions by skewed $\sin^2$ (0,0.3) and $\sin^2(0)$, respectively. Chemical shift and scalar J-couplings were obtained from (1).

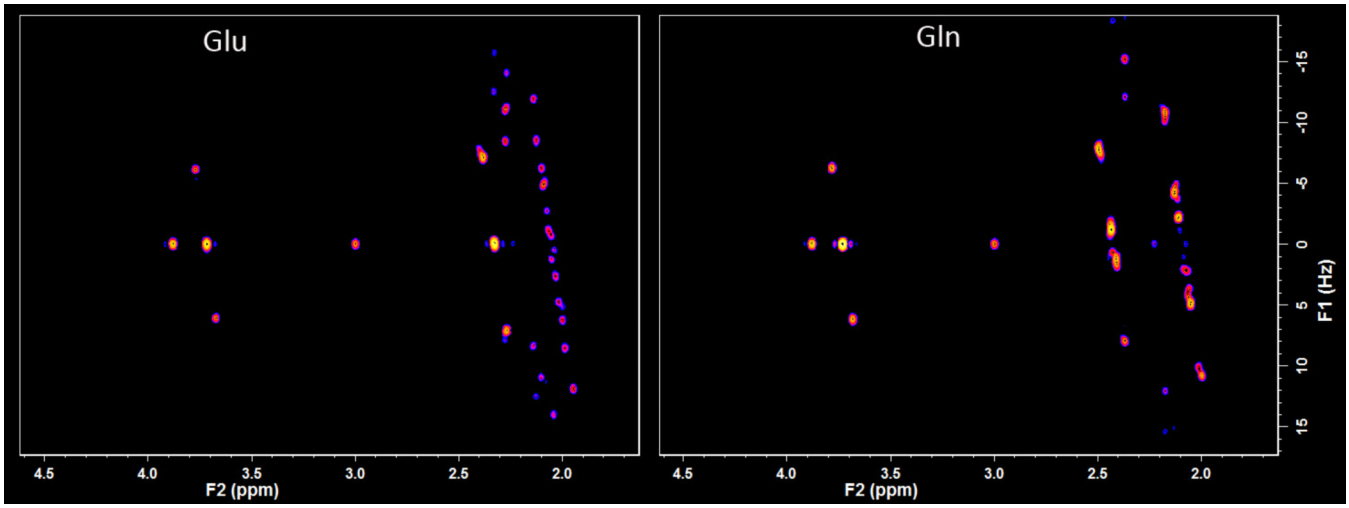

Figure 3.

Simulated J-resolved spectroscopy proton spectra of Glu and Gln with 5% Cr (at F1=0, F2=3.02 and 3.92ppm) at 3 Tesla. Notice the striking similarity of Glu and Gln structure and as a consequence, the spectral profiles. Spectra were simulated with 512 points in F2 and 200 points in F1 using a non-localized gradient JPRESS sequence (90° t1/2 G 180° t1/2 G Acquire, G: gradient pulse), with t1=20ms, F1 spectral width=50Hz, 128 F1 increments, F2 spectral width=7ppm. Processing was performed by zero filling to 2048 points in F2 and 512 points in F1, with skewed sin2 (0,0) and sin2(0) weighting along F2 and F1, respectively. Chemical shift and scalar J-couplings were obtained from (1).

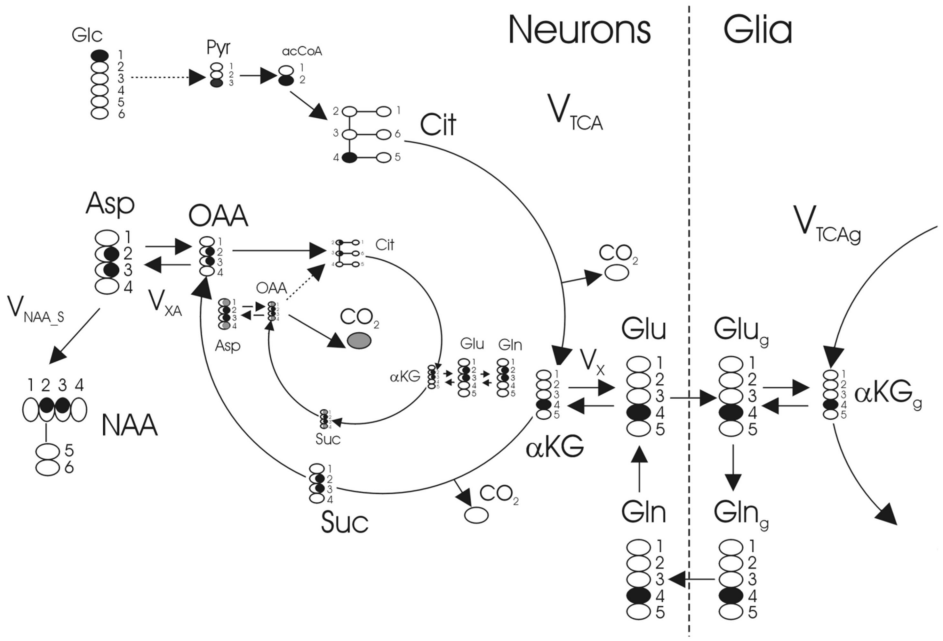

Figure 4.

Diagram of the TCA cycle and the Glu /Gln cycle in the neuron and glial cells as [1-^{13}C] glucose is metabolized. The filled circle indicates the carbon-13 label as it is metabolized through each turn of the cycle. The inner circle indicates the second turn of the TCA cycle and subsequent labeling of Glu and Gln.

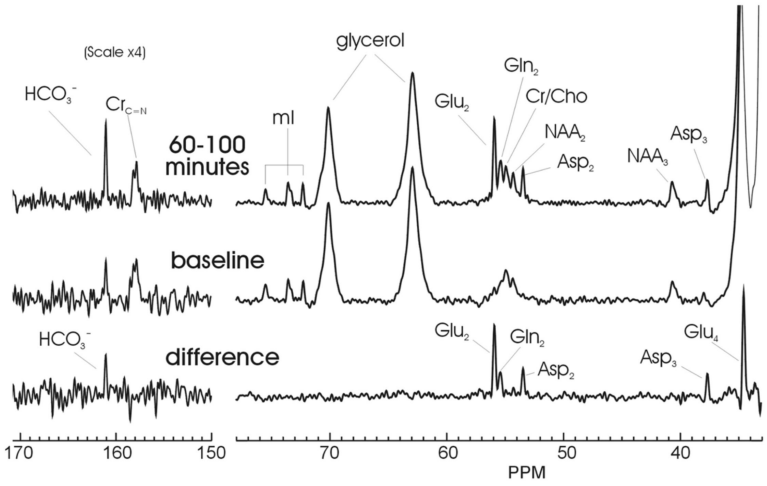

Figure 5.

Representative ^{13}C spectra obtained in healthy controls at 60-100 minutes after infusion (top), baseline (middle), and the difference spectra (bottom) that allows for the visualization of C2-Glu, Gln, and aspartate as well as C3-Asp and C4-glutamate which co-resonates with the natural abundance lipid signal and therefore only visualized upon subtraction.

Table 1

Glu and Gln concentration findings using various MRS techniques.

Method	TE(ms)/NS	Glu	Gln	Brain region, size	Bo (Tesla)	# of subjects[g]	Ref
PRESS TE-Ave	35-320/256 35-320/256	7.1±0.5[b] 11.7±1.1[b]	1.7±1.6[b] 3.2±1.6[b]	Left parietal WM, 8ml Mid-parietal GM, 8ml	3	6	(61)
PRESS TE-Ave MRSI	35/2	GM: 9.4±1.0 WM: 4.5 ±0.6	NA	Supratentorial, 1.8ml	3	3	(63)
Optimal TE (PRESS)[c]	80/128	ACC:11.7±1.2mM Hipp:10.9±1.4mM	ACC: 2.5±0.8mM Hipp: 2.2±0.8mM	ACC, 20ml Hipp, 12ml	3	40	(66)
Optimal TE (PRESS)	40/128	10.51±1.16mM 10.32±1.36mM	4.70±1.00mM 4.53±1.93mM	ACC, 4ml Insula, 4ml	1.5	21	(67)
Optimal TE PRESS	40/128	13.14 mM CRLB=8%	2.35 mM CRLB=29%	ACC, 12ml	3	6	(69)
Optimal TE STEAM	72/256 TM:6ms	10.00±0.69[d] CRLB:12.25±2.65	5.54±0.55[d] CRLB: 19.37±4.40%	MOP, 8ml	3	6	(70)
GluCEST[e] GRE	2.7/4	GM/WM:1.6±0.2	NA	Slice not reported	7	3	(72)
PRESS	16/100	WM:5.9 ± 0.5mM GM:9.4 ± 1.4mM	NA	Not reported, 4ml	7	3	(72)
STEAM-PR PRESS TE-Ave PRESS STEAM	6.5/256 30-180/256 40/256 72/256	1.12±0.08[a], CV=7.1% 1.01±0.09[a], CV=8.9% 1.09±0.13[a], CV=11.9% 1.23±0.17[a], CV=13.8%	0.33±0.08[a], CV=24.2% 0.28±0.13[a], CV=46.4 0.26±0.04[a], CV=15.4% 0.51±0.23[a], CV=45.1	ACG, 7.2ml	3	9	(74)
SPECIAL	6/128 6/64	8.9±0.9[b], CV=3±0.5 9.9±0.9[b], CV=1±0.5	1.6±0.4[b], CV=13±4.4 2.2±0.4[b], CV=4± 11	Occipital lobe, 8ml	3 7	6	(77)
SPECIAL	6/16-24	9.6±0.2[f]	2.3±0.1[f]	Primary visual cortex, 8.8ml	7	6	(85)
LASER	46/256	5.47±0.56mM 7.67±2.39mM	1.92±0.35mM 4.08±2.14mM	Parietal WM, 8ml Posterior Hipp, 1.7ml	4	10 8	(80)
STEAM (short TE)	6/160 TM:32ms	9.1 (CRLB<5%)[f]	3.3 (CRLB<5%)[f]	Occipital lobe, 8ml	7	10	(82)
STEAM (short TE)	8/128 8/128 8/128 8/256 8/512 8/128 8/128	9.8 (CRLB=2%)[f] 10.8 (CRLB=1.8%)[f] 7.3 (CRLB=2%)[f] 10.7 (CRLB=2.5%)[f] 5.9 (CRLB=9%)[f] 6.1 (CRLB=4.2%)[f] 10.5 (CRLB=2.2%)[f]	2.8 (CRLB=4%)[f] 3.3 (CRLB=4%)[f] 2.4 (CRLB=5%)[f] 3.4 (CRLB=7.5%)[f] Not reported 1.0 (CRLB=26%)[f] 4.0 (CRLB=4.8%)[f]	Occipital cortex, 8ml Posterior cingulate, 8ml Frontal WM, 8ml Putamen, 2.5ml Substantia nigra, 1ml Pons, 4ml Cerebral vermis, 6.2ml	7	14	(86)
Difference spectroscopy	73/256 73/384	1.16±0.10[a] 0.7±0.07[a]	NA	Anterior cingulate,7.3ml Cerebellar vermis,6.1ml	3	19	(90)
PRESS CPRESS TE-Ave	35/128 45/128 35-192.5/128	%CV=4.3,CRLB=7.4% %CV=5.2,CRLB=8.8% %CV=3.8,CRLB=6.3%	NA	PCG, 16ml	3	5	(97)
Spec-Selective Refocusing	128/64 158/128	9.7±0.5mM NA	NA 3.0±0.7mM	MPC, 22.5ml	3	7	(98)
PEPSI	15/8	9.8(CRLB=14.5%) 8.0(CRLB=12.2%)	4.1(CRLB=37%) 2.5(CRLB=24.1%)	Supraventricular slice, 1ml	3 4	9	(100)
Two-dimensional techniques							
J-resolved ProFit	31-229/ unknown	1.28 (CRLB=2.6±0.4%)[a]	0.21(CRLB=13.6±2.4%)[a]	Parietal lobe, 15.6ml	3	27	(112)

Method	TE(ms)/NS	Glu	Gln	Brain region, size	Bo (Tesla)	# of subjects[g]	Ref
JPRESS ProFit L-COSY ProFit	30-130/8 30-110/8	1.24±0.12[a],CRLB=2.52% 1.48±0.31[a],CRLB=1.42%	0.42±0.06[a],CRLB=6.6% 0.43±0.00[a],CRLB=18%	Occipital region, 27ml	3	8	(115, 146)
JPRESS PRESS	30-490/16 30/384	0.90±6%[a] 1.24±8%[a]	0.25±14%[a] 0.17±30%[a]	POC , 15.6ml	4	9[h]	(119)
Multi-TE J-resolved TE-Ave PRESS	30-180/16 30-180/16 30/256	1.11±0.11[a] (%CV=10.4) 0.86±0.15[a](%CV=16.4) 1.14±0.19[a] (%CV=16.9)	0.43±0.08[a] (%CV=18.3) 0.07±0.09[a] (%CV=n/a) 0.43±0.09[a] (%CV=19)	Precentral gyrus, 8ml	3	10[h]	(121)

[a] ratio to Cr,

[b] mmoles/kg wet weight,

[c] CSF corrected,

[d] Institutional units,

[e] Chemical exchange saturation transfer,

[f] μol/g,

[g] All subjects were healthy,

[h] Same subject scanned n times,

[i] Results were averaged across slice,

NS: Number of scans, ACC: Anterior cingulate cortex, Hipp: Hippocampus, MOP: Medial occipitoparietal, PR: phase-rotation, ACG: Anterior cingulate gyrus, PCG: Posterior cingulate gyrus, MPC: Medial prefrontal cortex, POC: Parieto-occipital cortex.